Mechanisms of Morphological Evolution on Faceted Core-Shell Nanowire Surfaces

Qian Zhang, Jean-Noël Aqua, Peter W. Voorhees, Stephen H. Davis

Mechanisms of Morphological Evolution on Faceted Core-Shell Nanowire Surfaces

Qian Zhang[a], Jean-Noël Aqua[b], Peter W. Voorhees[a,c], Stephen H. Davis[a,*]

[a] *Department of Engineering Sciences and Applied Mathematics, Northwestern University, 2145 Sheridan Road, Evanston, Illinois 60208-3125, USA*
[b] *Institut des Nanosciences de Paris, Université Pierre et Marie Curie Paris 6, UMR CNRS 7588, Paris, France*
[c] *Department of Materials Science and Engineering, Northwestern University, 2225 Campus Drive, Evanston, Illinois 60208-3030, USA*

Abstract

Core-shell nanowires with radial heterostructures hold great promise in photonic and electronic applications and controlling the formation of these heterostructures in the core-shell configuration remains a challenge. Recently, GaAs nanowires have been used as substrates to create AlGaAs shells. The deposition of the AlGaAs layer leads to the spontaneous formation of Al-rich stripes along certain crystallographic directions and quantum dots/wires near the apexes of the shell.

A general two-dimensional model has been developed for the motion of the faceted solid-vapor interfaces for pure materials that accounts for capillarity and deposition. With this model, the growth processes and morphological evolution of shells of nanowires around hexagonal cores (six small facets {112} in the corners of six equivalent facets {110}) are investigated in detail both analytically and numerically. It is found that deposition can yield facets that are not present on the Wulff shape. These small facets can have slowly time-varying sizes that can lead to stripe structures and quantum dots/wires depending on the balances between diffusion and deposition. The effects of deposition rates and polarity (or asymmetry) on planes {112} on the development of the configurations of nanowires are discussed. The numerical results are compared with experimental results giving almost quantitative agreement, despite the fact that only pure materials are treated herein whereas the experiments deal with alloys.

Keywords: core-shell nanowire growth, radial heterostructures, quantum dots/wires, deposition, diffusion
PACS: 81.05.Ea, 81.07.Gf, 81.10Aj

1. Introduction

Core-shell nanowires with radial heterostructures as building blocks for nanophotonics and nanoelectronics have attracted much attention due to their extended scaling to non-planar geometries and strong potential

*Corresponding author
Email addresses: qian.zhang_jennifer@northwestern.edu (Qian Zhang), aqua@insp.jussieu.fr (Jean-Noël Aqua), p-voorhees@northwestern.edu (Peter W. Voorhees), sdavis@northwestern.edu (Stephen H. Davis)

on improving the performance of photonic and electronic devices. Fig. 1(a) depicts the cross-section of one of the possible geometries of heterostructures in a "core-shell" system, consisting of a nanowire core surrounded by a shell of a different semiconductor material. Various research groups have synthesized and characterized GaAs-AlGaAs core-shell nanowires grown by both metal-organic vapour phase epitaxy (MOVPE) (Jiang et al., 2013; Wagner et al., 2010; Zheng et al., 2013) and molecular beam epitaxy (MBE) (Heiss et al., 2013; Rudolph et al., 2013). One of the most significant features of these heterostructures observed in the experiments is the formation of Al-rich {112} facets (in the corners of the six equivalent {110} side facets) which extend through the entire AlGaAs shell around the hexagonal GaAs core (Heiss et al., 2013; Jiang et al., 2013; Rudolph et al., 2013; Wagner et al., 2010; Zheng et al., 2013), see Fig. 1(a). Most core-shell nanowires observed in the experiments have six-fold symmetric structure about the nanowire axis. Nanowires with three-fold symmetric structures on the shell in which the lengths of facets $\{112\}_a$ and $\{112\}_b$ differ have been synthesized by Zheng et al. (2013). They indicate that it is the polarity of the surfaces that lead to a heterostructure shell with three-fold symmetry. Heiss et al. (2013) also present a quantum-dot-nanowire system in which the quantum dots form at the apexes of a GaAs/AlGaAs interface.

The mechanism of obtaining the lateral patterning of those nanostructures has been investigated in previous work (Biasiol et al., 2002; Shenoy, 2011; Xie et al., 1995). A widely accepted term "self-limiting" has been employed for decades (Biasiol et al., 2002; Heiss et al., 2013; Jiang et al., 2013; Rudolph et al., 2013; Wagner et al., 2010) to describe the ridge structure on the shell of the nanowire in experiments. A "self-limiting" profile of a facet in a certain direction is achieved when the length of the facet stays unchanged upon further growth while the lengths of facets in other directions still evolve in time. This self-limiting facet-size hypothesis has been invoked to explain the appearance of the facets {112} and the existence of stripes of enhanced Al concentration behind these facets in the AlGaAs alloy layer.

Here, a two-dimensional model inspired by the ideas of Carter et al. (1995) and Spencer et al. (2001) to describe the dynamic process of core-shell faceted nanowire growth of pure materials is developed. Focus is given to *pure-materials* in an effort to gain an understanding of the roles of capillarity and diffusion in setting the morphology of the growing shell. Despite this simplification, the model captures much of the essential physics governing the morphology of the growing shell, and the agreement between the calculated and measured shapes is very good. In our model, the growth rates of different facets in the shell depend on surface diffusion of adatoms driven by the surface gradient of chemical potential, the deposition of atoms and the surface energy of the facets.

Moreover, since GaAs/AlGaAs nanowire system is a coherent system without lattice misfit strain, only surface energy is considered in our model. However, if the system is strained, elastic energy has to be taken into account (see also Shenoy (2011), Vastola (2011)). In addition, as mentioned in Heiss et al. (2013), in the experiments, the GaAs core is first obtained at a given temperature. Then, the conditions are switched from axial to radial growth by increasing the As pressure and reducing the substrate temperature. Under

these conditions, there is negligible growth in the core in length. Thus, only the growth of the shell needed to be considered. Therefore, in this paper, we only investigate the growth of shell of nanowires in the radial direction. Also, in this continuous fully faceted model, the behaviour of each facets is counted in average. Thus, influence of different growth modes, such as layer-by-layer and step flow mentioned in Niu et al. (2012), on the facet morphology is beyond the discussion in this paper.

In order to have good comparison with experimental results, one focuses on the growth process and morphological evolution of the faceted shell on a hexagonal nanowire-core, see Fig. 1(a), but the model can describe the morphological evolution of faceted surfaces with any other configuration. In general, the facets with the lower surface energy are the ones with lower Miller indexes. This favors the formation of facets {110} in the shell. If only surface diffusion is considered, this should lead to a hexagonal core with sharp corners. However, if this trend could be opposed by deposition fluxes on facets, new facets may appear, such as facets {112}, that can lead to ridge structures and quantum dots/wires as shown in experiments.

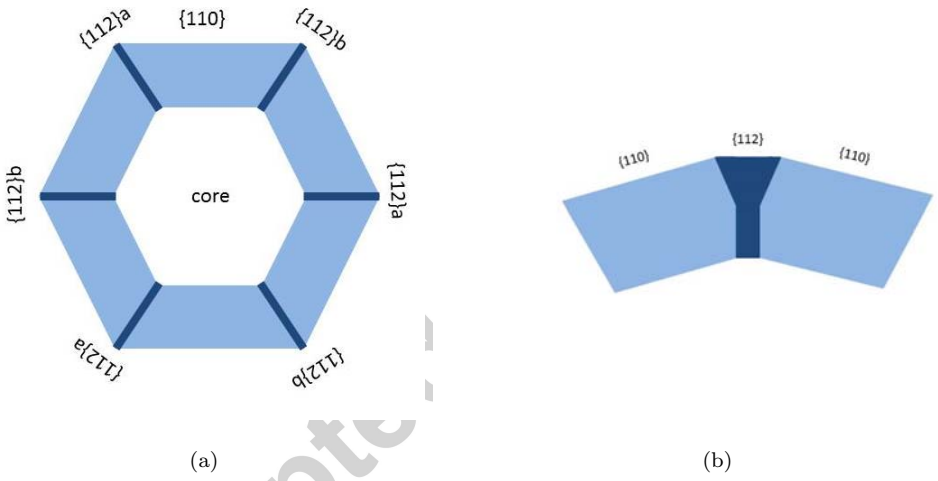

(a) (b)

Figure 1: (a) Schematic of a cross section of a nanowire with facets {112} along the corners of the hexagonal core. The nanowire-core is surrounded by a shell of different material. (b) Schematic of the "Y" shaped strips {112} formed in the corner of two neighboring equivalent side facets {110}.

We find that the lengths of facets {112} formed in the corners of the six equivalent facets {110} change slowly within a certain thickness of the shell (or a certain length of time) with deposition rates that are large enough to compete with surface diffusion. Afterwards, the lengths of facets {112} will increase rapidly. If the thickness of the shell is large enough (or the growth time is long enough), the final shape of the shell has six striped facets {112} formed in the corners of the six equivalent facets {110} with either a "Y" shape or a "V" shape, see Fig. 1(b). The areas in which the lengths of facets {112} increase rapidly can be identified as quantum dots/wires. The numerical and the experimental results agree quantitatively with reasonable choices of parameters. The configuration for the shell obtained in the numerical simulation, when

scaled, is almost identical to that obtained in Rudolph et al. (2013). This result differs from the traditional "self-limiting" state described in the literature.

Moreover, it can be shown analytically that there does not exist a "self-limiting" length on any facet in the dynamic process considered in this paper which implies that the lengths of facets {112} formed in the corners of the six equivalent facets {110} vary during the shell growth. This result follows from the continuity of chemical potential and surface diffusion flux in a quasi-static framework, at the points where two neighboring facets meet. These continuity conditions lead to the coupling of the lengths of facets {112}, lengths of facets {110} and other phenomenological coefficients, such as diffusion coefficients, in the expression for the normal velocity along each facet, which implies that the time evolution of length of each individual facet is influenced directly by the evolution of other facets.

Three types of configurations are found characterized by the striped shape in the direction {112} of the shell, i.e., hexagon, "Y" shape and "V" shape. The influences of deposition rates on the configurations of the shells are investigated in detail both analytically and numerically. Regimes of deposition rates and diameters of the cores generating different configurations of shells are also obtained numerically.

Furthermore, the influence of the polarity of facets $\{112\}_a$ and $\{112\}_b$ on the heterostructures in direction {112} of the shells is investigated both analytically and numerically. The polarity is introduced into the model by varying the lengths of facets {112} on the core, surface energies and diffusion coefficients on different facets. The results agree well with the conclusion that the polarity of the crystal structure drives the growth of core-shell heterostructure with a three-fold symmetry resulting in AlGaAs shells in Zheng et al. (2013).

The remainder of this paper is organized as follows. In Sec. 2, the derivation of the model is given in detail. Analytical results and numerical results are presented and discussed in Sec. 3 and Sec. 4, respectively. The paper concludes in Sec. 5.

2. Model

2.1. Model for shape evolution on faceted surfaces

A mathematical model is developed for the deposition of pure materials onto a faceted nanowire. For typical temperature and length scales, bulk diffusion is negligible relative to surface diffusion. It is assumed that the growth of each facet is due to the deposition of atoms from the vapor and surface-atoms diffusion from neighboring facets. It is further assumed that the crystal growth is sufficiently slow that any heat of crystallization diffuses much more quickly than the time scale for crystal growth so that the system remains isothermal.

To keep it simple, we only consider two-dimensional configuration in this paper. The surface of the solid material $\Gamma(t)$ is a closed curve. The morphological evolution of growing crystals is described in terms of the

velocity of the interface normal to itself, u_n. From mass conservation at the surface of the solid material, the surface evolves according to

$$u_n = -\Omega \nabla_s \cdot \mathbf{J}_s + f_n \qquad \text{on} \quad \Gamma(t), \tag{1}$$

where Ω is the atomic volume and f_n is the total deposition rate of the material in the outer normal direction of the surface $\Gamma(t)$. ∇_s is the surface gradient operator. The surface diffusion flux $\mathbf{J}_s$ is derived by second law of thermodynamics and Onsager's principle, giving

$$\mathbf{J}_s = -M \nabla_s \mu \qquad \text{on} \quad \Gamma(t), \tag{2a}$$

$$\mu = \nabla_s \cdot (\nabla_{\mathbf{n}} \gamma(\mathbf{n})) \qquad \text{on} \quad \Gamma(t) \tag{2b}$$

where $M > 0$ is the atom mobility and $\gamma(\mathbf{n})$ is the interfacial surface energy density. $\nabla_{\mathbf{n}}\gamma(\mathbf{n})$ is the variational derivative of $\int_{\Gamma(t)} \gamma(\mathbf{n}) \mathrm{d}\mathbf{S}$ with respect to $\mathbf{n}$. Derivation of the above model can be found in Cahn et al. (1996); Garcke (2013); Carter et al. (1997); Cermelli et al. (2005); Gurtin (2008); Stone (1990).

Because the faceted structure is a singular orientation, where the γ-plot has a cusp, the chemical potential of the facet cannot be calculated by (2b) directly. Alternatively, it can be related to surface energies only in an average sense over the facet, i.e, by considering

$$\bar{\mu}_i = \frac{\int_{L_i} \mu \mathrm{ds}}{L_i} \tag{3}$$

which defines the average chemical potential along facet i and L_i is the length of facet i. The average chemical potential which defines on each facet i can be can be related to the change in energy with respect to a virtual change of volume associated to the moving of a facet. In summary, we get the following formula of average chemical potential on facet i,

$$\bar{\mu}_i = \frac{1}{L_i}\left(\pm \frac{\gamma(\mathbf{n}_i)\mathbf{n}_i \cdot \mathbf{n}_{i+1} - \gamma(\mathbf{n}_{i+1})}{\sqrt{1-(\mathbf{n}_i \cdot \mathbf{n}_{i+1})^2}} \pm \frac{\gamma(\mathbf{n}_i)\mathbf{n}_i \cdot \mathbf{n}_{i-1} - \gamma(\mathbf{n}_{i-1})}{\sqrt{1-(\mathbf{n}_i \cdot \mathbf{n}_{i-1})^2}}\right). \tag{4}$$

Detailed derivation of Eq. (4) and the definition of "$\pm$" are shown in Appendix Appendix A. Notice that the formula of average chemical potential given in Eq. (4) is a more general formula compared with Eq. (1) and Eq. (2) in Carter et al. (1995).

We further assume that the normal velocity of a facet at any given time is a constant over the facet as the latter remains flat. This corresponds to the experimental findings in many core-shell nanowire growth processes, so that we will restrict to this hypothesis in the following.

The model for facet growth without deposition flux was first proposed in Carter et al. (1995). We consider only polygonal configurations which is a closed surface with N facets with lengths $L_0, L_1, \cdots, L_{N-1}$.

Therefore, for this faceted configuration, the shape-evolution model is as follows:

$$\bar{\mu}_i = \frac{\int_0^{L_i} \mu_i \mathrm{ds}}{L_i}, \tag{5a}$$

$$u_i(t) = -\Omega \partial_s J_s^i + f_i, \tag{5b}$$

$$J_s^i = -M_i \partial_s \mu_i \tag{5c}$$

together with the continuity conditions of surface diffusion flux and chemical potential at the corners,

$$\mu_{i+1}(0) = \mu_i(L_i), \tag{6a}$$

$$J_s^{i+1}(0) = J_s^i(L_i) \tag{6b}$$

for $i = 0, 1, 2, \cdots, N-1$, together with periodic boundary condition for surface diffusion flux and chemical potential at the end points, i.e.,

$$J_s^0(0) = J_s^{N-1}(L_N), \tag{7a}$$

$$\mu_0(0) = \mu_{N-1}(L_N). \tag{7b}$$

Moreover, the change of length with respect to time on each facet is

$$\frac{dL_i}{dt} = \pm \frac{u_{i+1} - \mathbf{n}_i \cdot \mathbf{n}_{i+1} u_i}{\sqrt{1 - (\mathbf{n}_i \cdot \mathbf{n}_{i+1})^2}} \pm \frac{u_{i-1} - \mathbf{n}_i \cdot \mathbf{n}_{i-1} u_i}{\sqrt{1 - (\mathbf{n}_i \cdot \mathbf{n}_{i-1})^2}} \tag{8}$$

for $i = 0, 1, 2, \cdots, N-1$, where the definition of $\pm$ is the same as that in Appendix A.

Notice that it is also possible that there is an additional diffusion barrier for corner crossing in some cases, which implies there exists unbalance in the diffusion fluxes at the corners. However, in this paper, we limit our discussions to the cases that the diffusion fluxes are continuous at the corners.

2.2. Dimensionless form of shape evolution model for faceted core-shell nanowires

In the following, consider the surface-shape evolution in the process of core-shell nanowire growth. We shall allow for the possibility that the cross-section of the core has six small facets {112} in the corners of six facets {110}, shown in Fig 2. The surface energy on facets {110} is γ_t whereas the surface energy on facets {112}sa and {112}sb are γ_{sa} and γ_{sb}, respectively. We first assume a three-fold symmetric geometrical structure in which the lengths of facets {112} are L_{sa} and L_{sb} alternating around the six corners, see Fig. 2. The length of facets {110} is L_t. In particular, the corresponding lengths of facets on the core are denoted by L_{ai}, L_{bi} and L_{ti}, respectively. Phenomena shown in the experiments suggest that one considers only nanowires with $L_{ti} \geq 10 \max\{L_{ai}, L_{bi}\}$. Then, the size of the core-shell nanowire with three-fold symmetric geometrical structure shown in Fig. 2 can be characterized by its diameter:

$$d \triangleq 2L_t + (L_{sa} + L_{sb}) \sec\theta.$$

Thus, the thickness of the shell is $T = (d - d_0)\cos\theta/2$, where d_0 is the diameter of the core.

In particular, if $L_{sa} = L_{sb}$, it is a six-fold symmetric geometrical structure. Moreover, the surface diffusion coefficient on facets $\{110\}$ is M_t and the surface diffusion coefficients on facets $\{112\}sa$ and $\{112\}sb$ are M_a and M_b, respectively. To obtain a dimensionless equation, we take the length (L_{bi}) of $\{112\}sb$ facets on the

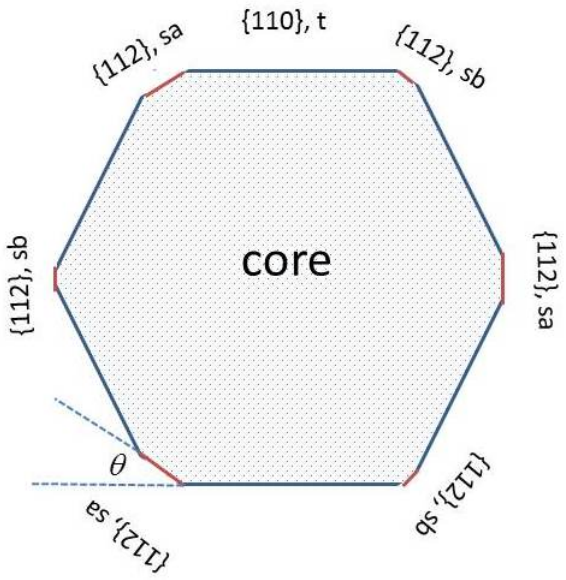

Figure 2: Schematic of cross-section of a core of a nanowire which is a three-fold symmetric structure with facets $\{112\}$ along the corners of the hexagonal core. The lengths of facets $\{112\}$ are L_{sa} and L_{sb} alternatively. In such structure, the angle θ between a facet $\{110\}$ and its neighboring facet $\{112\}$ is $\pi/6$.

core as the length scale L_0 and scale surface tensions by $\gamma_0 = -2\gamma_t \cot\theta + (\gamma_{sa} + \gamma_{sb})\csc\theta$. Without loss of generality, in the following $\gamma_0 > 0$, i.e., $(\gamma_{sa} + \gamma_{sb})/2\gamma_t > \cos\theta (\approx 0.8660)$. This implies that the length of facets $\{110\}$ does not equal to 0 in the equilibrium Wulff shape according to the Gibbs-Wulff theorem. Thus, the dimensionless lengths of the facets are $l_i = L_i/L_0$ for $i = 0, 1, 2, \cdots, 11$, the dimensionless form of the average chemical potential on each facet is $\bar{\mu}_{sa} = \lambda_a/l_{sa}$, $\bar{\mu}_{sb} = \lambda_b/l_{sb}$ and $\bar{\mu}_t = 1/l_t$, where

$$\lambda_a = \frac{1 - \frac{\gamma_{sa}}{\gamma_t}\cos\theta}{0.5(\frac{\gamma_{sa}}{\gamma_t} + \frac{\gamma_{sb}}{\gamma_t}) - \cos\theta}, \qquad \lambda_b = \frac{1 - \frac{\gamma_{sb}}{\gamma_t}\cos\theta}{0.5(\frac{\gamma_{sa}}{\gamma_t} + \frac{\gamma_{sb}}{\gamma_t}) - \cos\theta}. \tag{9}$$

Moreover, for simplicity, we take $6|(\lambda_1 + \lambda_2)|\Omega M_t \gamma_0 / L_0^3$ as velocity scale V_0. The dimensionless deposition rate on each facet is F_t, F_a and F_b, respectively. Here, $F_i = f_i/V_0$ for $i = t, a, b$. Physically, f_i/Ω is the deposition flux on facet i. Then, $f_i/\Omega = F_i(V_0/\Omega)$. Using the same symbols to represent the dimensionless

variables, the dimensionless equations are

$$\bar{\mu}_i = \frac{\int_0^{l_i} \mu_i \mathrm{ds}}{l_i}, \tag{10a}$$

$$u_i(t) = -\bar{\Omega}\partial_s J_s^i + F_i, \tag{10b}$$

$$J_s^i = -D_i \partial_s \mu_i \tag{10c}$$

together with the continuity conditions of surface diffusion flux and chemical potential at the joint points of neighboring facets as Eq. (6) and Eq. (7).

There are four dimensionless parameters, $\bar{\Omega} = \Omega/L_0^3$, $D_t = 1/[6\bar{\Omega}|(\lambda_a + \lambda_b)|]$, $D_a = M_a D_t/M_t$ and $D_b = M_b D_t/M_t$. In the next two sections, the relation between the dimensionless parameters of the model, such as deposition rates, surface tensions of different facets, lengths of facets on the core, surface-diffusion coefficients, and morphological evolution of the shell are investigated both analytically and numerically.

Remark 2.1. *In order to better illustrate the results and the dimensionless parameters mentioned in this paper, we give a set of reference parameters in experiments in the following.*

1. *We take the length (L_{bi}) of $\{112\}sb$ facets on the core as the length scale L_0. Typically, $L_0 = 2.5nm$ according to the experiments in Rudolph et al. (2013).*

2. *The surface energies are scaled by $\gamma_0 = -2\gamma_t \cot\theta + (\gamma_{sa} + \gamma_{sb})\csc\theta$. Typically, at $T = 660°C$, interfacial energy of a Al/vapour interface is $1.08Jm^{-2}$, approximately (Porter et al., 1981). If $\gamma_t = 1.08Jm^{-2}$ and $\gamma_{sa} = \gamma_{sb} = 3\gamma_t$, $\gamma_0 \approx 9.22Jm^{-2}$.*

3. *The velocity is scaled by $V_0 = 6|(\lambda_1 + \lambda_2)|\Omega M_t \gamma_0/L_0^3$. Typically, if $\gamma_{sa} = \gamma_{sb} = 3\gamma_t$ for Al/vapour interface at $T = 660°C$, $V_0 \approx 0.083Jm^{-2} \times M_t$ where $M_t = \Gamma_0 D/k_B T$ is the atom mobility coefficient on facet $\{110\}$. Here, k_B is the Boltzmann constant; T is growth temperature; Γ_0 is the surface density of adatoms; D is the surface diffusion coefficient on facet $\{110\}$.*

4. *For Al atoms or AlGaAs alloy, $\bar{\Omega} \approx 10^{-2} \sim 10^{-3}$, if $L_0 = 2.5nm$ as mentioned above. $D_t \approx 0.11 \times 10^2 \sim 0.11 \times 10^3$, if $\gamma_{sa} = \gamma_{sb} = 3\gamma_t$. Thus, $\bar{\Omega} D_t \approx 0.11$.*

3. Analytical results

The model in Sec. 2, gives the kinetic evolution

$$u_{sa} = \frac{12\bar{\Omega} D_a D_t}{l_{sa} A}[-\lambda_a(D_t l_{sb}^2 l_t + 2D_b l_{sb} l_t^2) - \lambda_b D_b l_{sa} l_t^2 + (D_t l_{sa} l_{sb}^2 + 3D_b l_{sa} l_t l_{sb})] + F_a, \tag{11a}$$

$$u_{sb} = \frac{12\bar{\Omega} D_b D_t}{l_{sb} A}[-\lambda_b(D_t l_{sa}^2 l_t + 2D_a l_{sa} l_t^2) - \lambda_a D_a l_{sb} l_t^2 + (D_t l_{sb} l_{sa}^2 + 3D_a l_{sb} l_t l_{sa})] + F_b, \tag{11b}$$

$$\begin{aligned} u_t = &\frac{6\bar{\Omega} D_t}{l_t A}[\lambda_a(D_a D_t l_{sb}^2 l_t + 3D_a D_b l_{sb} l_t^2) + \lambda_b(3D_a D_b l_{sa} l_t^2 + D_b D_t l_{sa}^2 l_t) \\ &- (D_a D_t l_{sa} l_{sb}^2 + 6D_a D_b l_{sa} l_t l_{sb} + D_b D_t l_{sb} l_{sa}^2)] + F_t \end{aligned} \tag{11c}$$

where $A = l_{sa}l_{sb}l_t(3D_aD_bl_t^2 + D_t^2 l_{sa}l_{sb} + 2D_aD_t l_{sb}l_t + 2D_bD_t l_{sa}l_t)$ and F_a, F_b and F_t are the normal velocities due to deposition (deposition rates).

Thus, in the following, we denote $v_{sa} = u_{sa} - F_a$, $v_{sb} = u_{sb} - F_b$ and $v_t = u_t - F_t$, actually, v_{sa}, v_{sb} and v_t are the normal velocities due solely to capillarity and diffusion. We also denote

$$f_{sa}(l_{sa}, l_{sb}, l_t) \triangleq -2v_{sa}\cot\theta + 2v_t\csc\theta, \tag{12a}$$

$$f_{sb}(l_{sa}, l_{sb}, l_t) \triangleq -2v_{sb}\cot\theta + 2v_t\csc\theta, \tag{12b}$$

$$f_t(l_{sa}, l_{sb}, l_t) \triangleq (v_{sa} + v_{sb})\csc\theta - 2v_t\cot\theta \tag{12c}$$

where f_{sa}, f_{sb} and f_t are tangential velocities (changing rates of the lengths) along the facets due solely to capillarity and diffusion. Denote

$$\Delta F_a \triangleq -2F_a\cot\theta + 2F_t\csc\theta, \tag{13a}$$

$$\Delta F_b \triangleq -2F_b\cot\theta + 2F_t\csc\theta, \tag{13b}$$

$$\Delta F_t \triangleq (F_a + F_b)\csc\theta - 2F_t\cot\theta \tag{13c}$$

where ΔF_a, ΔF_b and ΔF_t are tangential velocities (changing rates of the lengths) due to deposition. The time evolutions of lengths of each facet is eventually given by

$$\frac{dl_{sa}}{dt} = -2u_{sa}\cot\theta + 2u_t\csc\theta = \Delta F_a + f_{sa}(l_{sa}, l_{sb}, l_t), \tag{14a}$$

$$\frac{dl_{sb}}{dt} = -2u_{sb}\cot\theta + 2u_t\csc\theta = \Delta F_b + f_{sb}(l_{sa}, l_{sb}, l_t), \tag{14b}$$

$$\frac{dl_t}{dt} = (u_{sa} + u_{sb})\csc\theta - 2u_t\cot\theta = \Delta F_t + f_t(l_{sa}, l_{sb}, l_t) \tag{14c}$$

together with the initial conditions $l_{sa}(0) = l_{ai}$, $l_{sb}(0) = 1$ and $l_t(0) = l_{ti}$. This a system of nonlinear ordinary differential equations. There are four sets of dimensionless parameters: the initial configuration, i.e., the initial lengths of the facets, l_{ai}, $l_{bi}(= 1)$ and l_{ti}, the ratios of surface energies of facets, i.e., γ_{sa}/γ_t and γ_{sb}/γ_t, the ratios of surface-diffusion coefficients on facets, i.e., D_a/D_t, D_b/D_t, the deposition rates of facets, i.e., F_a, F_b and F_t.

Eq. (11) and Eq. (14) clearly show the competition between capillary effects (v_{sa}, v_{sb} and v_t in Eq. (11) and f_{sa}, f_{sb} and f_t in Eq. (14)) and depostion effects (F_a, F_b and F_t in Eq. (11) and ΔF_a, ΔF_b and ΔF_t in Eq. (14)). In the following, we consider two limiting cases.

a. Equilibrium Wulff shapes (in the absence of deposition):. By the model above, the equilibrium Wulff shape is found in the absence of deposition, i.e., $F_a = F_b = F_t = 0$. For example, a six-fold symmeteric structure in which $\gamma_{sa} = \gamma_{sb} = \gamma_s$, i.e., $\lambda_a = \lambda_b \triangleq \lambda$, $D_a = D_b \triangleq D_s$, $l_{ai} = l_{bi} \triangleq l_{si}$ implies $l_{sa} = l_{sb} \triangleq l_s$ according to Eq. (14). By Eq. (11) and (14), if $\lambda > 0$ which implies $\cos\theta(\approx 0.8660) < \gamma_s/\gamma_t < \sec\theta(\approx 1.1547)$, the equilibrium Wulff shape is a do-decagon with $l_s/l_t = \lambda$. If $\lambda \le 0$, which implies $\gamma_s/\gamma_t \ge \sec\theta(\approx 1.1547)$,

the equilibrium Wulff shape is a hexagon. These results are consistent with the conclusions of Gibbs-Wulff theorem. As suggested in the paper of Zheng et. al.Zheng et al. (2013), if $\gamma_s/\gamma_t = 3$, then $\lambda \approx -0.7489 < 0$. Therefore, in the remainder of this paper, it is always assumed that $\lambda_a \leq 0$ and $\lambda_b \leq 0$, i.e., the equilibrium Wulff shape is a hexagon in the six-fold symmetric structures. This implies $\gamma_t \leq \min\{\gamma_{sa}, \gamma_{sb}\}\cos\theta$.

Remark 3.1. *Notice that $l_s = 0$ or $l_t = 0$ will introduce a singularity in the expressions of dl_s/dt and dl_t/dt; generally speaking, our model does not deal with the cases in which any of the facets disappear or nucleate as time evolves, but does not violate the energy law when $\lambda < 0$(or $\gamma_s/\gamma_t > \sec\theta$) in which the equilibrium Wulff shapes are hexagons because*

$$\frac{dE}{dt} = 6\gamma_s\frac{dl_s}{dt} + 6\gamma_t\frac{dl_t}{dt} < 0$$

when $l_s \geq 0$ and $l_t \geq 0$ according to Eq. (14).

b. Deposition only (in the absence of diffusion):. If $\Delta F_a \neq 0$, $\Delta F_b \neq 0$ and $\Delta F_t \neq 0$ and $D_a = D_b = 0$ which implies $f_{sa} = f_{sb} = f_t = 0$, then

$$\frac{dl_{sa}}{dt} = \Delta F_a, \quad \frac{dl_{sb}}{dt} = \Delta F_b, \quad \frac{dl_t}{dt} = \Delta F_t. \tag{15}$$

If any of $\Delta F < 0$, in other words, if the deposition rate on one facet is too large compared with the deposition rates of its neighboring facets, that facet will disappear as time evolves. For simplicity, in the rest of this paper, unless specified, we consider only cases in which $l_{sa}, l_{sb}, l_t > 0$ and $\Delta F_a > 0$, $\Delta F_b > 0$ and $\Delta F_t > 0$, i.e., $\max\{F_a, F_b\}\cos\theta < F_t < \min\{F_a, F_b\}\sec\theta$ and $1 \leq \max\{F_a, F_b\}/\min\{F_a, F_b\} < 4/3$ which implies the deposition rates on the facets are in the same order. Under this assumption, the shells always have twelve facets (in the absence of capillarity).

Under the assumptions mentioned above, investigations will be made on the competition between deposition and capillarity which yields facets that are not present on the equilibrium Wulff shape (hexagon). In addition, investigation will also be made on how configurations on the shells, observed in the experiments, are introduced by the balance of deposition and diffusion/capillarity.

3.1. Influence of polarity of sa and sb facets on the configurations of the shell

In this section, the influence of polarity (or asymmetry) on facets {112} on the evolution of the configuration of the shell at early times is investigated. The polarity is introduced by varying the lengths of facets {112} on the core (geometrical polarity), surface energies or diffusion coefficients (material polarity) on different facets. Since the introduction of polarity influences only the capillarity effect, i.e., f_{sa}, f_{sb} and f_t in Eq. (14), for simplicity, in this section, it is always assumed that $F_a = F_b \triangleq F_s$, i.e, $\Delta F_a = \Delta F_b \triangleq \Delta F_s$.

3.1.1. Different lengths of sa and sb on the core, $l_{ai} \neq l_{bi}$

In this section, consider a case in which $\gamma_{sa} = \gamma_{sb} \triangleq \gamma_s$ which implies $\lambda_a = \lambda_b \triangleq \lambda$, $D_a = D_b \triangleq D_s$. Therefore, as enforced by Eq. (14),

$$\frac{d}{dt}(l_{sa} - l_{sb}) = \frac{D_s D_t \bar{\Omega} \alpha}{l_{sa} l_{sb} A}(l_{sa} - l_{sb}) \tag{16}$$

where $\alpha = (D_t l_{sa}^2 l_{sb} + 3D_s l_{sa} l_{sb} l_t + D_t l_{sa} l_{sb}^2) - \lambda(2D_s l_{sa} l_t^2 + 2D_s l_{sb} l_t^2 + D_t l_{sa}^2 l_t + D_t l_{sb}^2 l_t + D_t l_{sa} l_{sb} l_t) > 0$ so that, if $l_{ai} > l_{bi}$, l_{sa} is always larger than l_{sb} during time evolution and vice versa. Also, by (16), the state in which $l_{sa} = l_{sb}$ is not a stable state which implies that small perturbations on the lengths of *sa* and *sb* will lead to unsymmetrical shell structures in the nanowire, even though initially the core has a six-fold symmetrical geometrical structure.

Moreover, according to Eq. (14),

$$\frac{d}{dt}(\frac{l_{sa}}{l_{sb}}) = \frac{1}{l_{sb}}(\frac{dl_{sa}}{dt} - \frac{l_{sa}}{l_{sb}}\frac{dl_{sb}}{dt}) = \frac{1}{l_{sb}}(1 - \frac{l_{sa}}{l_{sb}})(\Delta F_s + 2v_t \csc\theta - 2\delta\cot\theta) \tag{17}$$

where $\delta = 12D_s D_t \bar{\Omega}[-\lambda(D_t l_{sa}^3 l_t + D_t l_{sb}^3 l_t + 2D_s l_{sa}^2 l_t^2 + 2D_s l_{sb}^2 l_t^2 + 3D_s l_{sa} l_{sb} l_t^2 + D_t l_{sa} l_{sb}^2 l_t + D_t l_{sa}^2 l_{sb} l_t) + (D_t l_{sa}^3 l_{sb} + D_t l_{sa} l_{sb}^3 + 3D_s l_{sa} l_{sb}^2 l_t + 3D_s l_{sa}^2 l_{sb} l_t + D_t l_{sa}^2 l_{sb}^2)]/(l_{sa} l_{sb} A) > 0$. Notice that the sign of $(\Delta F_s + 2v_t \csc\theta - 2\delta\cot\theta)$ can change during time evolution. Therefore, if initially the lengths of *sa* and *sb* are different, the ratio between the lengths of *sa* and *sb* can either tend to 1 or away from 1 with time. However, according to Eq. (16), l_{sa} can not be equal to l_{sb} even for long time. Therefore, if $l_{ai} \neq l_{bi}$, the final configuration of the shell can not be a six-fold symmetric structure.

3.1.2. Different diffusion coefficients on sa and sb, $D_a \neq D_b$

In this section, we consider another case in which $l_{ai} = l_{bi} \triangleq l_{si}$, $\gamma_{sa} = \gamma_{sb} \triangleq \gamma_s$ which implies $\lambda_a = \lambda_b \triangleq \lambda$ whereas $D_a \neq D_b$. According to Eq. (14), we have

$$\frac{d}{dt}\frac{l_{sa}}{l_{sb}} = -2\cot\theta\bar{\Omega}(D_a - D_b)\frac{12D_t^2 l_{sa} l_{sb}(l_{sb} - \lambda l_t)}{l_{sb}^2 A} + O(\frac{l_{sa}}{l_{sb}} - 1). \tag{18}$$

This implies that if $D_a > D_b$, then $l_{sb} > l_{sa}$ at early times when $l_{ai} = l_{bi}$. Therefore, different diffusion coefficients on the *sa* and *sb* facets will lead to three-fold symmetric shells even though $\gamma_{sa} = \gamma_{sb}$ and $F_a = F_b$ and the core of the nanowire is six-fold symmetric geometrical structure.

3.1.3. Different surface tensions on sa and sb, $\gamma_{sa} \neq \gamma_{sb}$

In this section, we consider another case in which $l_{ai} = l_{bi} \triangleq l_{si}$, $D_a = D_b \triangleq D_s$ whereas $\gamma_{sa} \neq \gamma_{sb}$. According to Eq. (14), we have

$$\frac{d}{dt}\frac{l_{sa}}{l_{sb}} = \frac{24\cot\theta D_s D_t \bar{\Omega}}{l_{sb}^2}\frac{(\lambda_a - \lambda_b)}{l_{sb}(D_t l_{sb} + 3D_s l_t)} + O(\frac{l_{sa}}{l_{sb}} - 1). \tag{19}$$

This implies that if $\gamma_{sa} > \gamma_{sb}$, then $\lambda_a < \lambda_b$ so that $l_{sb} > l_{sa}$ at early times when $l_{ai} = l_{bi}$. Therefore, different surface tensions on *sa* and *sb* will lead to three-fold symmetric shells even though $D_a = D_b$, $F_a = F_b$ and the core of the nanowire is a six-fold symmetric geometrical structure.

3.2. Kinetic Wulff shapes (Deposition-dominant dynamic processes)

In this section, we investigate the long-time behavior of the growth of the shell. First, consider two possible deposition-dominant dynamic processes

B 1. Low temperatures, where it is easy to deposit but surface diffusion is small:
$D_a, D_b, D_t \ll 1$, with all other parameters of order 1.

B 2. On the core, the length of facets {110} is much larger than the lengths of facets {112}:
$l_{ti} \gg 1$, $l_{ai} \simeq 1$ and $l_{bi} = 1$ with all other parameters of order 1. Applying a Taylor expansion with respect to $1/l_t$ on u_{sa}, u_{sb} and u_t according to Eq.(11), we get

$$u_{sa} = F_a - \frac{4D_t\bar{\Omega}}{l_{sa}l_{sb}}\frac{\lambda_b l_{sa} + 2\lambda_a l_{sb}}{l_{sa}}\frac{1}{l_t} + O(\frac{1}{l_t})^2, \tag{20a}$$

$$u_{sb} = F_b - \frac{4D_t\bar{\Omega}}{l_{sa}l_{sb}}\frac{\lambda_a l_{sb} + 2\lambda_b l_{sa}}{l_{sb}}\frac{1}{l_t} + O(\frac{1}{l_t})^2, \tag{20b}$$

$$u_t = F_t + \frac{6D_t\bar{\Omega}}{l_{sa}l_{sb}}(\lambda_b l_{sa} + \lambda_a l_{sb})(\frac{1}{l_t})^2 + O(\frac{1}{l_t})^3. \tag{20c}$$

The shell thickness along the nominal direction of {110} facets is defined as T,

$$\frac{dl_{sa}}{dT} \approx \frac{\Delta F_a}{F_t} = 2\csc\theta(1 - \frac{F_a}{F_t}\cos\theta), \tag{21a}$$

$$\frac{dl_{sb}}{dT} \approx \frac{\Delta F_b}{F_t} = 2\csc\theta(1 - \frac{F_b}{F_t}\cos\theta), \tag{21b}$$

$$\frac{dl_t}{dT} \approx \frac{\Delta F_t}{F_t} = 2\csc\theta(\frac{F_a + F_b}{2F_t} - \cos\theta). \tag{21c}$$

Thus, because $\Delta F_a > 0$, $\Delta F_b > 0$ and $\Delta F_t > 0$, for T large enough,

$$\frac{l_{sa}}{l_{sb}} \approx \frac{\Delta F_a}{\Delta F_b}, \quad \frac{l_{sa}}{l_t} \approx \frac{\Delta F_a}{\Delta F_t}, \qquad \frac{l_{sb}}{l_t} \approx \frac{\Delta F_b}{\Delta F_t}. \tag{22}$$

Notice that in the dynamic dominant processes, the diffusion is still present, even though it is small compared with deposition. Thus, $l_{sa} : l_{sb} : l_t$ approaches $\Delta F_a : \Delta F_b : \Delta F_t$ when T is large enough.

Remark 3.2. *In particular,* $[l_{sa}(T) - l_{sa}(0)]/T \le 2\csc\theta(1 - F_a\cos\theta/F_t)$ *and* $[l_{sb}(T) - l_{sb}(0)]/T \le 2\csc\theta(1 - F_b\cos\theta/F_t)$ *because* $dl_{sa}/dT \le \Delta F_a/F_t$ *and* $dl_{sb}/dT \le \Delta F_b/F_t$. *Thus, the average rates of change of* l_{sa} *and* l_{sb} *within thickness* T *are small, if* $(1 - F_a\cos\theta/F_t)$ *and* $(1 - F_b\cos\theta/F_t)$ *are small, i.e.,* $F_a/F_t \lesssim \sec\theta$ *and* $F_b/F_t \lesssim \sec\theta$. *Later, this conclusion is useful in the analysis of the formation of ridge structures in which facets* {112} *have a slowly time-dependent size in the shell of the nanowire.*

Configurations satisfying Eq. (22) are quasi-stationary kinetic shapes which are generated in the kinetic-dominant processes. This is the so-called "kinetic Wulff shape". Notice that the kinetic Wulff shape is not simply given by the magnitude of the fluxes impinging on different facets, but deposition rates weighted by the angles between the facets. Thus, for example, if $F_a : F_t : F_b = 1.1 : 1 : 1.1$, in the kinetic Wulff shape,

$l_{sa} : l_t : l_{sb}$ approaches to $\Delta F_a : \Delta F_t : \Delta F_b = 0.2024 : 1 : 0.2024$. Moreover, kinetic Wulff shapes are scale independent, or self-similar according to the discussion above.

More generally, according to Eq. (14), $f_t > 0$ and $dl_t/dt > 0$ because $\lambda_a < 0$, $\lambda_b < 0$ and $\Delta F_t > 0$. Moreover, if $D_a/D_t \geq \sec\theta/3$ and $D_b/D_t \geq \sec\theta/3 (\approx 0.3849)$, the capillary effects on the facets, expressed as $|f_{sa}|$, $|f_{sb}|$ and $|f_t|$ in Eq. (14), are monotonically decreasing functions with respect to l_{sa}, l_{sb} and l_t. Therefore, if there exists a time t^* such that $dl_{sa}/dt > 0$ and $dl_{sb}/dt > 0$ at $t = t^*$, then $dl_{sa}/dt > 0$ and $dl_{sb}/dt > 0$ for $t > t^*$ because $\Delta F_a > 0$ and $\Delta F_b > 0$. Moreover, $|v_t|$ is also a monotonically decreasing function of l_{sa}, l_{sb} and l_t. Therefore, in such cases, if $u_t > 0$ at t^*, when thickness of the shell T is large enough, one can also get the kinetic Wulff shapes.

3.3. Non-existence of self-limiting facet sizes

For simplicity, we only consider cases in which $l_{ai} = l_{bi} \triangleq l_{si}$, $\gamma_{sa} = \gamma_{sb} \triangleq \gamma_s$ which implies $\lambda_a = \lambda_b \triangleq \lambda$ and $D_a = D_b \triangleq D_s$ and $F_a = F_b \triangleq F_s$. Therefore, according to Eq. (17), during growth of the shell, $l_{sa} = l_{sb} \triangleq l_s$ and we consider only cases in which $l_s > 0$. This implies, $u_{sa} = u_{sb} \triangleq u_s$ and there are only two evolution equations to consider, one for the {110} facets and one for the {112} facets,

$$u_s = \frac{1}{l_s}\frac{12 D_s D_t \bar{\Omega}(l_s - \lambda l_t)}{l_s l_t (D_s l_t + D_t l_s)} + F_s, \tag{23a}$$

$$u_t = -\frac{1}{l_t}\frac{12 D_s D_t \bar{\Omega}(l_s - \lambda l_t)}{l_s l_t (D_s l_t + D_t l_s)} + F_t. \tag{23b}$$

Therefore, using Eq. (14),

$$\frac{dl_s}{dt} = -2u_s\cot\theta + 2u_t\csc\theta = \Delta F_s - \frac{24 D_s D_t \bar{\Omega}\csc\theta(l_s - \lambda l_t)(l_t\cos\theta + l_s)}{l_s^2 l_t^2 (D_s l_t + D_t l_s)}, \tag{24a}$$

$$\frac{dl_t}{dt} = 2u_s\csc\theta - 2u_t\cot\theta = \Delta F_t + \frac{24 D_s D_t \bar{\Omega}\csc\theta(l_s - \lambda l_t)(l_s\cos\theta + l_t)}{l_s^2 l_t^2 (D_s l_t + D_t l_s)} \tag{24b}$$

where $\Delta F_s = -2F_s\cot\theta + 2F_t\csc\theta$ and $\Delta F_t = 2F_s\csc\theta - 2F_t\cot\theta$. In the following, we show by contradiction that there does not exist self-limiting lengths for facets.

Suppose there exists a self-limiting length for the facets {112} denoted by l_s^{sl} for $t \geq t_0$, i.e.,

$$\frac{dl_s}{dt} = \Delta F_s - \frac{24 D_s D_t \bar{\Omega}\csc\theta(l_s^{sl} - \lambda l_t)(l_t\cos\theta + l_s^{sl})}{(l_s^{sl})^2 l_t^2 (D_s l_t + D_t l_s^{sl})} = 0, \qquad t \geq t_0. \tag{25}$$

This implies,

$$\Delta F_s (l_s^{sl})^2 l_t^2 (D_s l_t + D_t l_s^{sl}) - 24 D_s D_t \bar{\Omega}\csc\theta(l_s^{sl} - \lambda l_t)(l_t\cos\theta + l_s^{sl}) = 0. \tag{26}$$

Eq. (26) is a third-order polynomial with respect to l_t so there exist at most three zeroes (or specific values of l_t which yield a time independent l_t). However, since there are fixed values of l_t, the latter can not change, i.e, $dl_t/dt = 0$ for $t \geq t_0$ and $l_t = l_t^{sl}$. Otherwise, dl_s/dt is not equal to 0 for $t \geq t_0$. Therefore, we have proved that there does not exist the so-called "self-limiting" length for facets {112}, i.e., there does

not exist cases in which $dl_s/dt = 0$ and $dl_t/dt \neq 0$ after a certain time. Similarly, we can prove that there does not exist "self-limiting" length for facets $\{110\}$, i.e., there does not exist cases in which $dl_t/dt = 0$ and $dl_s/dt \neq 0$ after a certain time.

Moreover, according to the above discussion, suppose the evolution of the lengths of the facets stops at $t = t_0$ with $l_s = l_s^{sl}$ and $l_t = l_t^{sl}$. Therefore,

$$\frac{dl_s}{dt} = \Delta F_s - \frac{24 D_s D_t \bar{\Omega} \csc\theta (l_s^{sl} - \lambda l_t^{sl})(l_t^{sl}\cos\theta + l_s^{sl})}{(l_s^{sl})^2 (l_t^{sl})^2 (D_s l_t^{sl} + D_t l_s^{sl})} = 0, \quad t \geq t_0 \tag{27a}$$

$$\frac{dl_t}{dt} = \Delta F_t + \frac{24 D_s D_t \bar{\Omega} \csc\theta (l_s^{sl} - \lambda l_t^{sl})(l_s^{sl}\cos\theta + l_t^{sl})}{(l_s^{sl})^2 (l_t^{sl})^2 (D_s l_t^{sl} + D_t l_s^{sl})} = 0. \quad t \geq t_0 \tag{27b}$$

We solve the above equation system and obtain

$$\frac{l_s^{sl}}{l_t^{sl}} = -\frac{F_t}{F_s}, \tag{28}$$

which implies there does not exist $l_s^{sl} > 0$ and $l_t^{sl} > 0$ because $F_t > 0$ and $F_s > 0$. This conclusion is natural because it is not possible to have l_s and l_t constants, as there is growth in the thickness of the shell and thence the perimeter must increase.

In summary, there does not exist the so called "self-limiting" length on any facet during time evolution in the six-fold configurations. Also, there does not exist the stable state in which $dl_s/dt = 0$ and $dl_t/dt = 0$ at the same time in the present of deposition rates on all the facets. Therefore, according to the argument before, the shell of the nanowire grows all the time so that all the lengths l_s and l_t can not be constant. Similarly, we can also prove that there does not exist the "self-limiting" length on any facet in three-fold configurations.

4. Numerical results

In this section, some numerical simulation results investigating the growth processes of the shells of core-shell nanowires are presented.

In the six-fold symmetric core-shell nanowire growth, the initial lengths of facets sa and sb are equal, i.e, $l_{ai} = l_{bi} \triangleq l_{si}$ and $l_{si} = 1$, the deposition rates on facets sa coincide with the deposition rates on facets sb, i.e., $F_a = F_b \triangleq F_s$, the surface energies on facets $\{112\}sa$ and $\{112\}sb$ are equal to each other, i.e., $\gamma_{sa} = \gamma_{sb} \triangleq \gamma_s$ and $\lambda_a = \lambda_b \triangleq \lambda$, the surface diffusion coefficients on different facets are equal to each other, i.e, $D_a = D_b = D_t \triangleq D$. Moreover, as suggested in the paper of Zheng et. al.Zheng et al. (2013), $\gamma_s/\gamma_t = 3$. Thus, $D\bar{\Omega} = 0.1113$ according to the choice of scaling parameters in Sec. 2.2.

Under the assumptions mentioned above, suppose $F_s = RF_t$ where the deposition rate on facets $\{110\}$ is F_t and the dimensionless length of the facets $\{110\}$ on the core is l_{ti}. According to the assumption in Sec. 2.2, $l_{ti} \geq 10$. The dimensionless diameter of the core is $d_0 = 2l_{ti} + 2\sec\theta$ ($\approx 2l_{ti}$ when l_{ti} is large enough).

Therefore, the problem has been reduced to three parameters R(or F_s), F_t and l_{ti} (or d_0) which govern the growth process of the shell of six-fold symmetric core-shell nanowires.

Moreover, for both three-fold and six-fold symmetric structures, we introduce a parameter $\mathcal{N}$ according to Eq. (20) and only consider cases $\Delta F_a = \Delta F_b \triangleq \Delta F_s > 0$,

$$\mathcal{N} = \frac{48 D_t \bar{\Omega} \max\{|\lambda_a|, |\lambda_b|\} \cot\theta}{(d_0 + 2T \sec\theta)\Delta F_s},$$

where T is the thickness of the shell and $(d_0 + 2T\sec\theta)$ is the diameter of the core-shell nanowire, to estimate the relative importance of diffusion with respect to deposition on facets {112}. Under the assumptions mentioned above, when $\mathcal{N} \approx 1$, the evolution of the configuration depends on the balance of diffusion and deposition; when $\mathcal{N} \ll 1$, diffusion is negligible compared with deposition; when $\mathcal{N} \gg 1$, the diffusion effect is dominant.

4.1. Comparison with experiments

4.1.1. Ridge Structures

Consider the six-fold symmetric core-shell nanowire growth of Rudolph et al. (2013). According to their experimental data, the diameter of the core is $70nm \pm 10nm$, the thickness of the shell is $25nm \pm 0.2nm$, the thickness of the striped facets {112} is $2.5nm \pm 0.5nm$. Therefore, in the numerical simulation, we take $l_{ti} = 13.0$, $F_s = 1.43$ and $F_t = 1.3$ (see Simulation #2.1 in Table 1). With parameters mentioned above, the kinetic Wulff shape is a "self-similar" do-decagon with $l_s/l_t \approx \Delta F_s/\Delta F_t (= 0.2024)$ according to the analytical results. In the numerical result, l_s is in the range of 0.9647 ± 0.08 (see the figure embedded in Fig.4(a)) for thickness of the shell (T) from $T = 0$ to $T = 9.7238$. Thus, the configuration for the shell obtained in numerical simulation has quantitative agreement with the experimental results in Rudolph et al. (2013) upon scaling the results to the case used in the experiments (see Fig. 3(a)). However, the length of the side facet begins to increase once T exceeds approximately 10, (see Fig. 3(b)).

Evolution of l_s and l_t with respect to thickness of the shell is shown in Fig. 4(a). Both Fig. 4(a) and the figure embedded in it show that the lengths of both facets {112} (l_s) and facets {110} (l_t) vary during the whole growth process, even though within small thickness of the shell, say $0 \le T \le 9.7238$, the rate of change of l_s is small compared with that of length of facets {110}. Therefore, while we observe a relatively time independent l_s over a range of core thicknesses, there does not exist a "self-limiting" facet length for the configuration considered here, consistent with the analysis above.

In Fig. 4(b), when T is small and $\mathcal{N} \approx 1$, because of the competition between diffusion and deposition, l_s/l_t first decreases to a minimun value before it increases. When the thickness of the shell (T) is large enough which implies that $\mathcal{N} \ll 1$, the final shape of the shell is six stripes {112} formed in the corners of the six equivalent side facets {110} with "Y" shapes (see Fig. 3(b)) while l_s/l_t approaches to 0.2 which is close to the ratio given by the kinetic Wulff shape (see Fig. 4(b)).

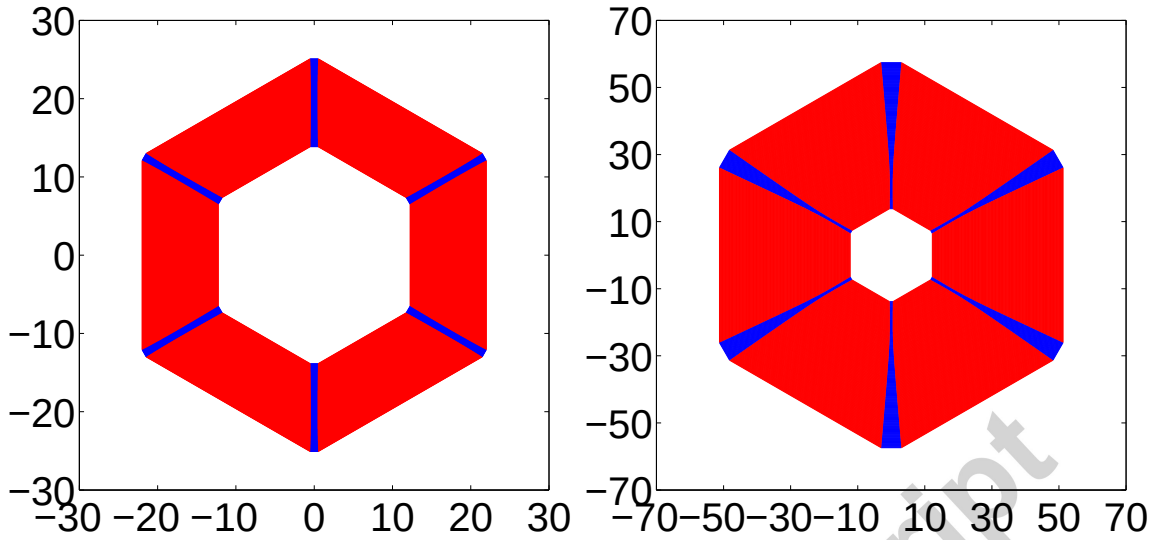

(a) (b)

Figure 3: Cross-section of the six-fold core-shell nanowire with six facets {112} (blue color) along the corners of six facets {110} (red color) in Simulation #2.1. (a) The ridge structure along direction {112} in the configuration of the shell of the nanowire for thickness of the shell (T) increases from $T = 0$ to $T = 9.7238$. (b) The "Y" structure along direction {112} for thicker shells, specifically when the thickness of the shell (T) increases from $T = 0$ to $T = 38.96$.

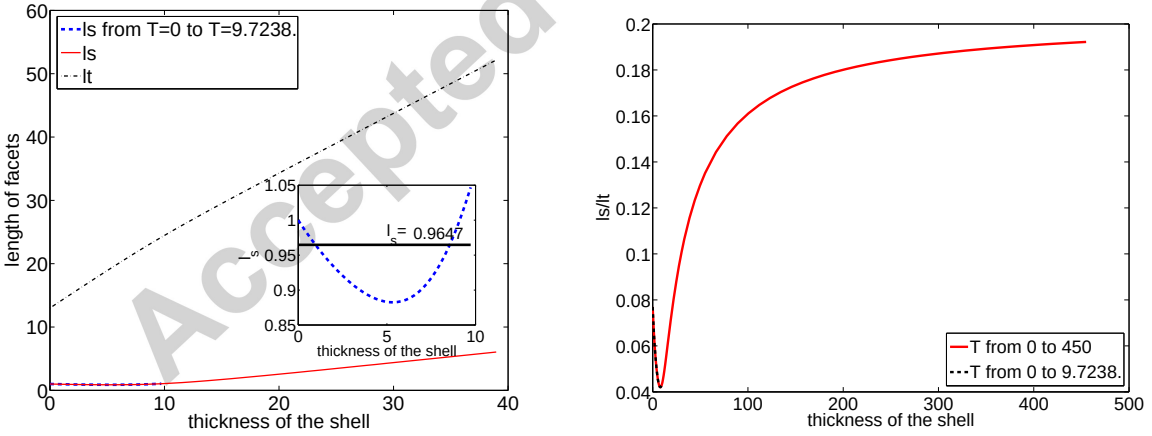

(a) (b)

Figure 4: (a) Evolution of $l_t[L_0]$ and $l_s[L_0]$ with respect to thickness of shell ($T[L_0]$) in Simulation #2.1. The figure embedded shows evolution of l_s with respect to thickness of the shell (T) from $T = 0$ to $T = 9.7238$; (b) Evolution of l_s/l_t with respect to thickness of the shell ($T[L_0]$) in Simulation #2.1.

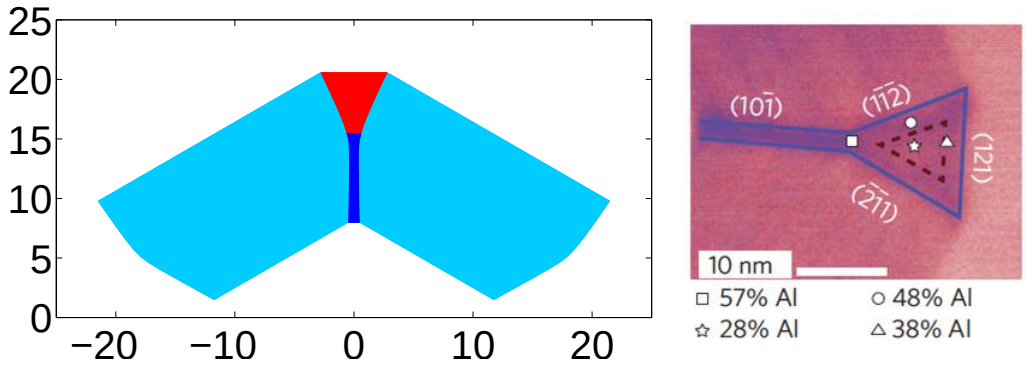

(a) (b)

Figure 5: (a) This is partial view of configuration of cross section of the shell of six-fold core-shell nanowire with one facet {112} (dark blue and red) along the corner of two neighbouring facets {110} (light blue). (b) Detail of Al-poor quantum dot/wire located within the fork-like Al-rich stripes obtained by Heiss et. al. in Heiss et al. (2013). (Figure courtesy Heiss et al. (2013))

4.1.2. Quantum Dots/Wires

In this part, we take $F_s = 0.287$ and $F_t = 0.319$ and the other parameters are the same as in Simulation #2.1 (see Simulation #2.4 in Table 1) in order to correspond to the experiments of Heiss et al in Heiss et al. (2013). In this case we find shell configurations that are consistent with the formation of the quantum dots/wires at the edge of the shell (see Fig. 5(a)). Compared with the configuration of Al-poor quantum dot/wire obtained by Heiss et.al. in Heiss et al. (2013) shown in Fig. 5(b), our numerical simulation is in qualitative agreement with the experimental result. Moreover, employing the same notations on the facets for the ratio of the facet lengths as shown in Fig. 5(b), we have

$$l_{(10\bar{1})} : l_{(1\bar{1}\bar{2})} : l_{(\bar{2}\bar{1}1)} : l_{(121)} : l_{si} = 7.54 : 5.47 : 5.47 : 5.54 : 1$$

in the numerical simulation result shown in Fig. 5(a) which is very close to that seen experimentally.

4.2. Influence of deposition rates

If $\Delta F_s \leq 0$ i.e. $F_s \geq F_t \sec\theta$, according to Eq. (23) and Eq. (24), $dl_s/dt < 0$ under the assumption of $\lambda < 0$. In this case, the configuration of the shell is a hexagon. Indeed, we take $F_s = 1.16F_t$ and $F_t = 1$ as a representative case and other parameters are taken the same as in Sec. 4.1.1 (see Simulation #2.2 in Table 1). The shell obtained by the numerical simulation is a hexagon (see Fig. 6(a)) and evolution of l_s and l_t with respect to the thickness of the shell is shown in Fig. 7(a). Similarly, when $\Delta F_t < 0$, the configuration of the shell is also a hexagon. Therefore, in the following, we only discuss cases in which $\cos\theta < F_s < F_t \sec\theta$, i.e., $\Delta F_s > 0$ and $\Delta F_t > 0$.

Moreover, due to Eq. (14), for $l_t \gg 1$ and $l_s \sim O(1)$,

$$\frac{dl_s}{dt} = \Delta F_s - 2\cot\theta(-\frac{12D\bar{\Omega}\lambda}{l_s^2 l_t}) + O(\frac{1}{l_t})^2, \tag{29a}$$

$$\frac{dl_t}{dt} = \Delta F_t + 2\csc\theta(-\frac{12D\bar{\Omega}\lambda}{l_s^2 l_t}) + O(\frac{1}{l_t})^2. \tag{29b}$$

In order to have the ridge structures suggested in the experiments, one would expect that at early times of growth $dl_s/dt \approx 0$ and $\Delta F_t > 0$, i.e, $F_s > F_t\cos\theta$. Moreover, l_s/l_t tends to $\Delta F_s/\Delta F_t$ for large shell thicknesses (or very long times) according to the analytical results in Sec. 3.2. Therefore, rough estimate of dl_s/dt and dl_t/dt suggests that $\Delta F_s < \Delta F_t$, i.e, $F_s > F_t$, in order to have $l_s < l_t$ in the kinetic Wulff shapes.

Hence, according to the discussion above, the influence of the deposition rates breaks up into two intervals with respect to F_s and F_t, i.e, (i) $F_t\cos\theta < F_s \leq F_t$ (i.e. $\Delta F_s \geq \Delta F_t > 0$), (ii) $F_t < F_s < F_t\sec\theta$ (i.e. $0 < \Delta F_s < \Delta F_t$).

Generally speaking, we get three configurations of the shells characterized by the striped shape in the direction {112} as follows:

1. **Hexagonal**: The final configuration of the shell is a hexagon which implies that all the facets {112} disappear as time increases (See configuration in Fig. 6(a)).
2. **"Y" shape with ridge structures**: For a given thickness (T_0) of the shell,

$$V(T_0) \triangleq \frac{1}{2}[\max_{0\leq T\leq T_0} l_s(T) - \min_{0\leq T\leq T_0} l_s(T)], \quad L(T_0) \triangleq \frac{1}{2}[\max_{0\leq T\leq T_0} l_s(T) + \min_{0\leq T\leq T_0} l_s(T)].$$

   We define the configuration of the shell as a *"ridge" structure* from the core (See the configuration in Fig. 3(a)), if within a certain thickness (T_0) of the shell, $V/L \leq 30\%$ and $L/T_0 \leq 15\%$. As the shell gets thicker, the lengths of facets {112} increase much faster. If the thickness of the shell is large enough, the lengths of facets {112} are much larger than the lengths of facets {112} on the core. We define the configuration of the shell with features mentioned above as "Y" shape with ridge structures (See configuration in Fig. 3(b)).
3. **"V" shape**: The lengths of facets {112} increase rapidly with respect to the thickness of the shell. In other words, the final configuration does not consist of a ridge structure satisfying the definition mentioned above and the lengths of facets {112} are not equal to 0 (See configuration in Fig. 6(b)).

4.2.1. $\cos\theta < F_s \leq F_t$ *(or* $0.866 < R \leq 1$*)*

Take $F_s = 0.9F_t$ and $F_t = 1$ as a representative case for $F_s \leq F_t$ and other parameters are taken the same as in Sec. 4.1 (see Simulation #2.3 in Table 1). The shell obtained by numerical simulation is shown in Fig. 6(b) and evolution of l_s and l_t with respect to thickness of the shell (T) is shown in Fig. 7(b). Therefore, one can see that the facets {112} have "V" shapes on the shell, i.e, the lengths of facets {112}

Table 1: Dimensionless parameters taken in the numerical simulations in Sec. 4.2

Sim.	$F_s[V_0]$	$F_t[V_0]$	$l_{si}[L_0]$	$l_{ti}[L_0]$	$D\bar{\Omega}$	γ_s/γ_t
#2.1	1.43	1.3	1	13	0.1113	3
#2.2	2.32	2.0	1	13	0.1113	3
#2.3	0.90	1.0	1	13	0.1113	3
#2.4	0.287	0.319	1	13	0.1113	3
#2.5	1.17, 1.43[a]	1.3	1	13	0.1113	3

[a] $F_{s1} = 1.43$ for $T \leq 4.21$, $F_{s1} = 1.17$ for $T > 4.21$ whereas deposition rates on other facets {112} are 1.43.

increase rapidly at early times (see Fig. 7(b)). Because $\mathcal{N} \approx 0.3$ on the core and $\mathcal{N}$ decreases as T increases, during the whole growth process and so, deposition dominates diffusion.

Moreover, when $F_s \leq F_t$, one gets two types of configurations only, hexagonal and "V" shapes. In the following, the influence of deposition rates on the configurations of the shell is studied. For simplicity, we take $F_s = 0.9F_t$. The problem has been reduced to two parameters F_t and l_{ti} (or d_0 because $l_{ti} = d_0/2 - \sec\theta$) which govern the growth process of the shell. The numerical results are summarized in Fig. 8. The blue line in the figure is $F_t = 3.9/l_{ti}$ obtained by substituting the parameters above into leading-order terms of Eq. (29a) and letting $\Delta F_s - 2\cot\theta(-12D\bar{\Omega}\lambda/l_{si}^2 l_{ti}) = 0$. Therefore, $\mathcal{N}(t=0) \approx 1$ which implies a balance between diffusion and deposition. The red stars are obtained numerically. Given a value of the initial length of the facets {110} (l_{ti}), the star above the blue line shows the critical value of F_t for transition from a hexagonal shell to a shell with "V" shape in the direction {112}. The dashed line is obtained by cubic spline interpolation at the values of stared data points.

In summary, if (l_{ti}, F_t) is taken from the region (shaded blue in Fig. 8) enclosed by the dashed line, the horizontal and vertical axes, the final configuration of the shell of the nanowire is hexagonal. If (l_{ti}, F_t) is located on or above the dashed line, there are "V" shapes in the {112} direction as shown in Fig. 8.

4.2.2. $F_t < F_s < F_t \sec\theta$ (or $1 < R < 1.155$)

We take $F_s = 1.1F_t$ as a representative case for $F_t < F_s < F_t\sec\theta$; one numerical example with $F_t = 1.3$ and $F_s = 1.43$ of this case has been shown in Sec. 4.1.1. Moreover, in the following, the influence of deposition rates and diameters of the cores on the configurations of the shells is studied. Suppose $F_s = RF_t$ and $R \in (1, \sec\theta)$ ($\sec\theta \approx 1.1547$).

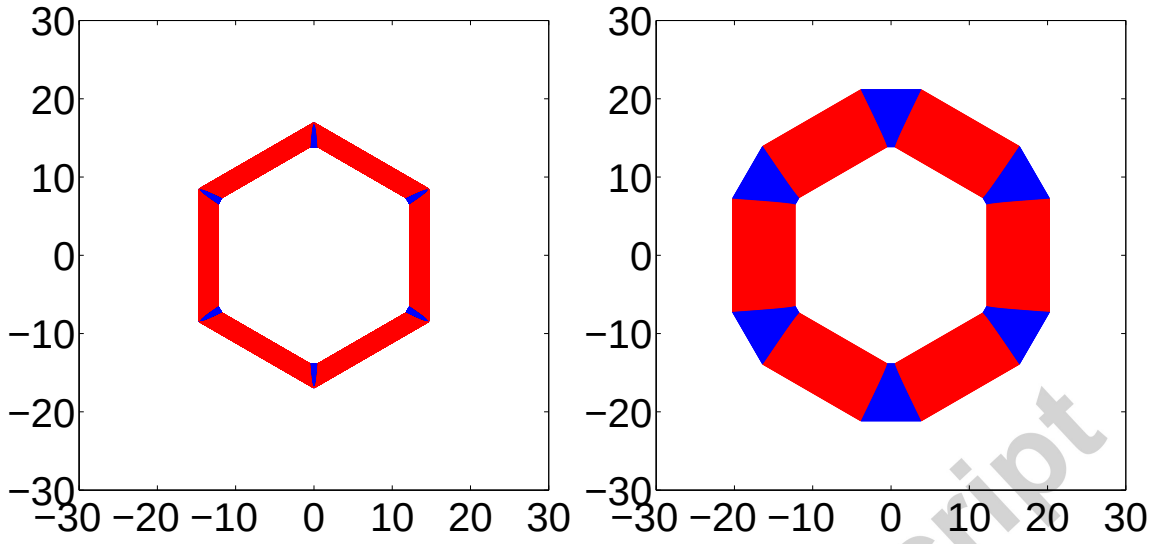

(a) (b)

Figure 6: Cross-section of the six-fold core-shell nanowire with six facets {112} (blue color) along the corners of six facets {110} (red color). (a)Hexagonal configuration of core-shell nanowire obtained in Simulation #2.2 in which $F_s = 1.16F_t (F_s > F_t/\cos\theta)$; (b) "V"-shape configuration of core-shell nanowire obtained in Simulation #2.3 in which $F_s = 0.9F_t (F_s < F_t)$.

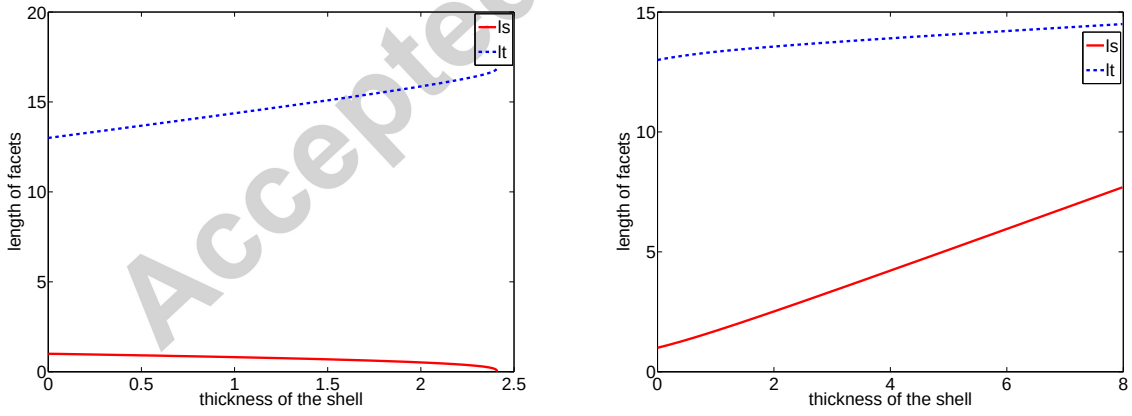

(a) (b)

Figure 7: Evolution of $l_t[L_0]$ and $l_s[L_0]$ with respect to thickness of the shell ($T[L_0]$). (a) Numerical results obtained in simulation #2.2. (b) Numerical results obtained in Simulation #2.3.

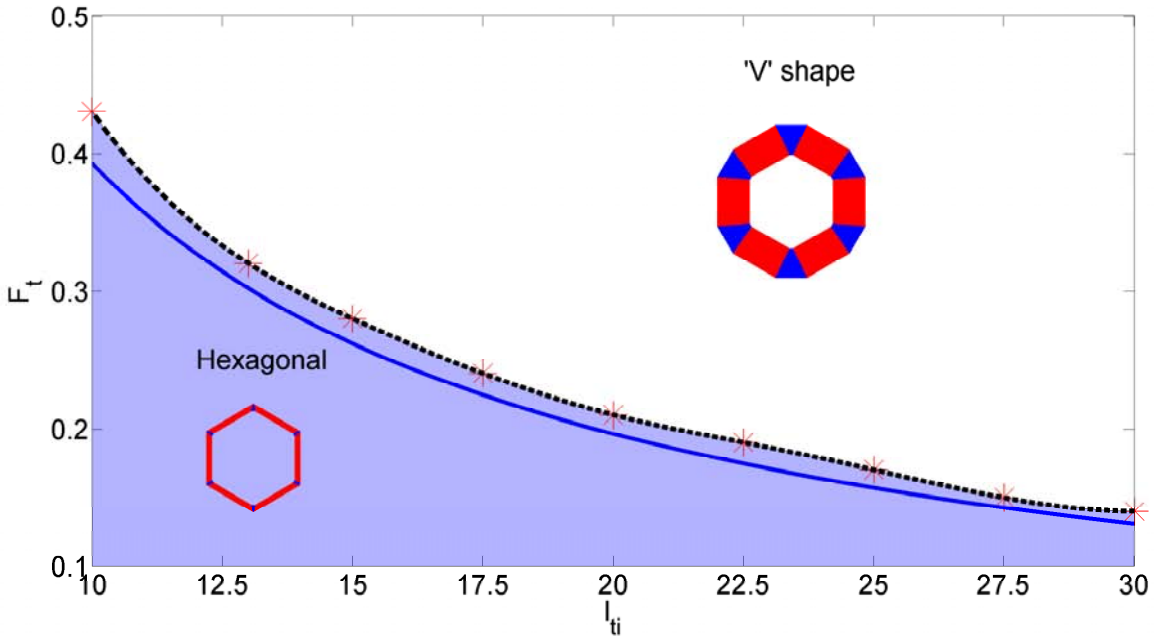

Figure 8: Configuration map for $l_{si} = 1[L_0]$, $D\bar{\Omega} = 0.1113$ and $F_s = 0.9F_t$, depending on the deposition rate on facets {110} $F_t[V_0]$ and the length of the facets {110} on the core $l_{ti}[L_0]$. The blue line is $F_t = 3.9/l_{ti}$. The red stars are obtained numerically. The dashed line is obtained by cubic-spline interpolation at the values of stars. The blue line is the analytical approximation of the dashed line.

(i) $R = 1.1$

If $R = 1.1$, the numerical results are summarized in Fig. 9. The blue line in the figure is $F_t = 18.2/l_{ti}$ which is obtained by substituting the parameters above into leading-order terms of Eq. (29a) and letting $\Delta F_s - 2\cot\theta(-12D\bar{\Omega}\lambda/l_{si}^2 l_{ti}) = 0$ which implies $\mathcal{N}(t=0) \approx 1$. The red stars are obtained numerically. Given a value of the dimensionless length of the facets $\{110\}$ on the core (l_{ti} or d_0 because $d_0 = 2(l_{ti} + \sec\theta)$), the star below the blue line shows the critical value of F_t for transition from a hexagonal shell to a shell with ridge structure whereas the star above the blue line shows the critical value of F_t for transition from a shell with ridge structure in the direction $\{112\}$ to a shell with "V" shape. The dashed line is obtained by cubic spline interpolation at the values of stars.

In summary, if (l_{ti}, F_t) lies in the area (shaded grey in Fig. 9) between the dashed lines, nanowires of "Y" shape with ridge structures are obtained. If (l_{ti}, F_t) is in the region (shaded blue in Fig. 9) enclosed by the lower dashed line and the horizontal and vertical axes where $\mathcal{N}(t=0) > 1$, the final configuration of the shell is hexagonal. Moreover, if (l_{ti}, F_t) is located above the upper dashed line where $\mathcal{N}(t=0) < 1$, there are facets $\{112\}$ with "V" shapes on the shell. The results are easy to understand by considering a fixed initial length of the top facet. For small deposition rate on the facets $\{110\}$ (F_t) , the faster growing facets $\{112\}$ disappear. As F_t increase, a balance between deposition and diffusion is obtained that yields a slowly time dependent length of the facets $\{112\}$. At still faster deposition rates, the length of the slower growing facets $\{112\}$ is never constant.

(ii) $R = 1.15$

In order to investigate the influence of ratio of F_s/F_t (or F_s) on the configuration of the shell, we take $F_s = 1.15F_t$ as another representative case for $F_t < F_s < F_t/\cos\theta$ and other parameters are taken the same as the cases in which $F_s = 1.1F_t$. The numerical results are summarized in Fig. 10. The blue line in the figure is $F_t = 212/l_{ti}$ which is obtained by substituting the parameters above into leading-order terms of Eq. (29a) and letting $\Delta F_s - 2\cot\theta(-12D\bar{\Omega}\lambda/l_{si}^2 l_{ti}) = 0$. The red stars are obtained numerically. Given a value of l_{ti} (or d_0 because $d_0 = 2(l_{ti} + \sec\theta)$), the star below the blue line shows the critical value of F_t for transition from a hexagonal shell to a shell with ridge structures. The dashed line is obtained by cubic spline interpolation at the values of stars.

In summary, if (l_{ti}, F_t) is taken from the region (shaded blue in Fig. 10) enclosed by the dashed line, the horizontal and the vertical axes, the configuration of the shell is hexagonal. If (l_{ti}, F_t) is located above the dashed line (shaded grey in Fig. 10), we have facets $\{112\}$ with "Y" shapes in the shell.

4.2.3. The effect of a fluctuation of deposition rate on a single facet resulting a quantum dot/wire

Inspired by the numerical results mentioned above, we also study a geometry where a single facet is affected by fluctuations. This geometry is dedicated to experiments which reveal a quantum dot/wire on a

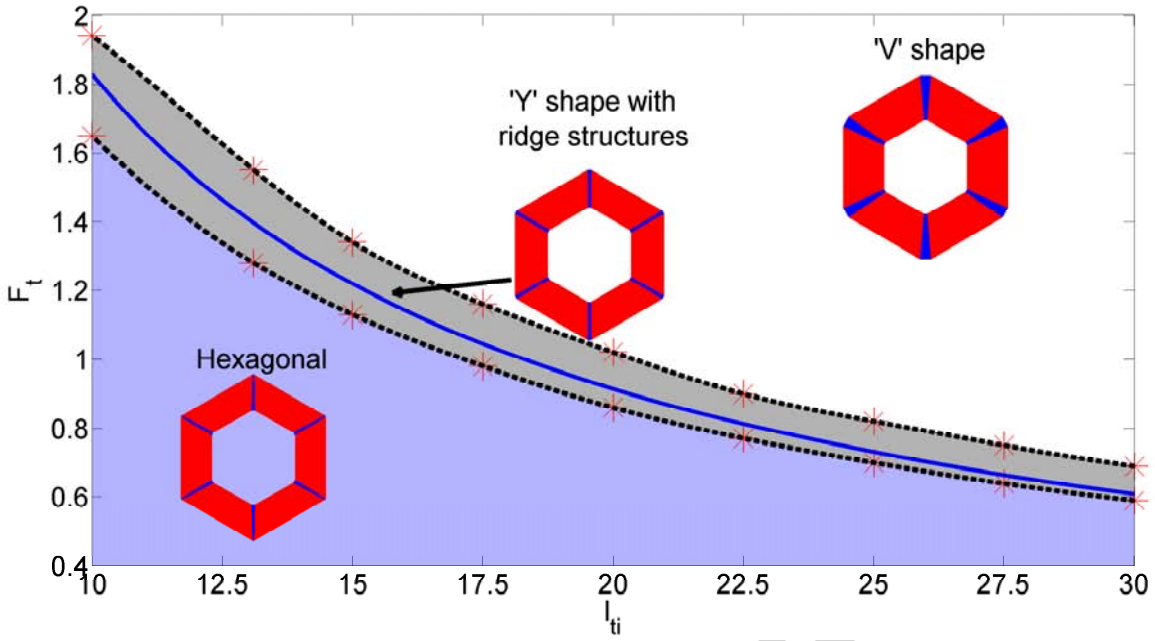

Figure 9: Configuration map for $l_{si} = 1[L_0]$, $D\bar{\Omega} = 0.1113$ and $F_s = 1.1F_t$, depending on the deposition rate on facets {110} $F_t[V_0]$ and the length of the facets {110} on the core $l_{ti}[L_0]$. The blue line is $F_t = 18.2/l_{ti}$. The red stars are obtained numerically. The dashed line is obtained by cubic spline interpolation at the values of stars.

single edge, where the symmetry is no longer six-fold.

We first take $F_t = 1.3$ and $F_s = 1.43$ ($F_s = 1.1F_t$) and other parameters are taken the same as in Sec. 4.1.1 when the thickness of the shell $T \leq 4.21$ (see Simulation #2.5 in Table 1). We denote the facet on the top as facet $s1$ (see Fig. 11(a)) and the deposition rate on this facet as F_{s1}. For $T > 4.21$, F_{s1} is decreased to 1.17 ($F_{s1} = 0.9F_t$) whereas deposition rates on the other facets are kept as 1.43. We find that the fluctuation on F_{s1} results in the formation of a quantum dot/wire in the direction {112} where facet $s1$ is located while the configurations of the shell in the other directions do not change significantly (see Fig. 11(a)). Denoting facets starting from facet $s1$ clockwise as $s1, t1, s2, t2, s3, t3, s4, t4, s5, t5, s6, t6$ respectively, evolution of lengths of these facets with respect to thickness of the shell (thickness in $t2$ direction) is shown in Fig. 11(b). In the numerical result, one can see that before $T = 4.21$, the configuration of the shell is a six-fold symmetric structure while after $T = 4.21$, the configuration of the shell clearly breaks the six-fold symmetry and becomes a two-fold symmetric structure because of the introduction of fluctuation on the deposition rates on facet $s1$.

4.2.4. Summary

According to the numerical results on the six-fold symmetric core-shell nanowire growth, under the assumption that $\gamma_s/\gamma_t \geq \sec\theta(\approx 1.155)$ and the lengths of facets {110} are larger or equal to ten times of

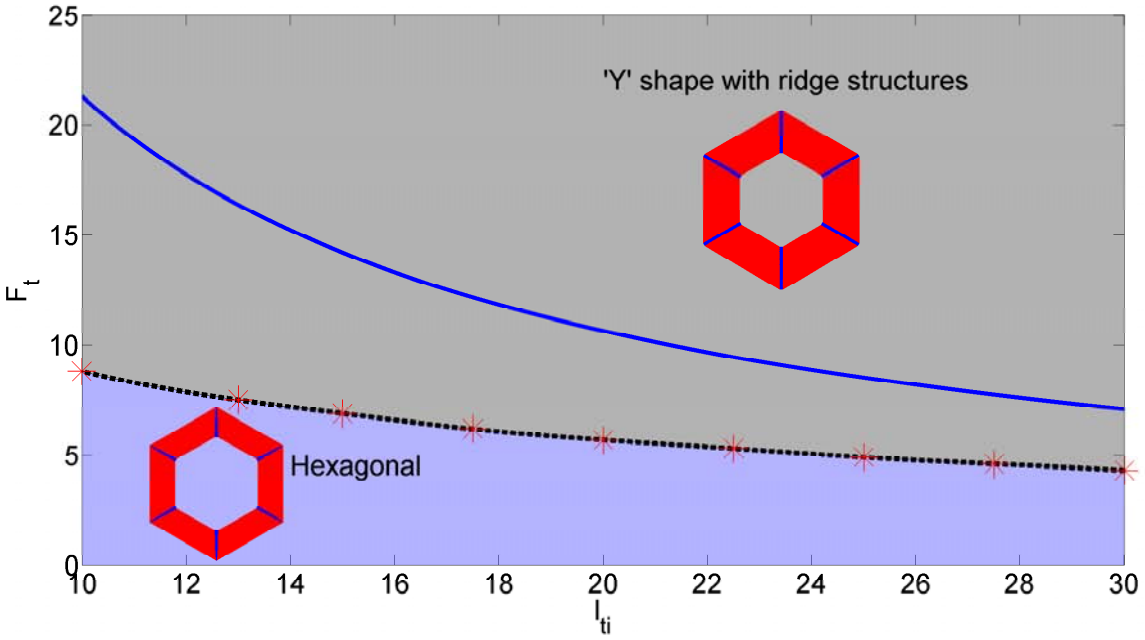

Figure 10: Configuration map for $l_{si} = 1[L_0]$, $D\bar{\Omega} = 0.1113$ and $F_s = 1.15F_t$, depending on the deposition flux on {110} facets $F_t[V_0]$ and the length of the {110} facets on the core $l_{ti}[L_0]$. The blue line is $F_t = 212/l_{ti}$. The red stars are obtained numerically. The dashed line is obtained by cubic-spline interpolation at the values of stars. Notice that, if $F_t \in (0, \infty)$, the blue line is a good approximation of the dotted line.

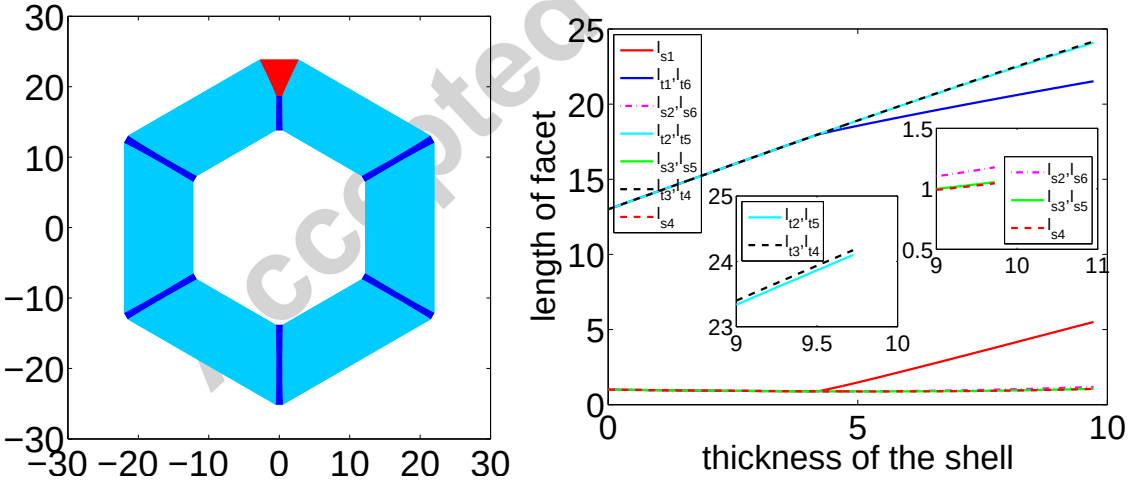

(a) (b)

Figure 11: (a) Configuration of core-shell nanowire obtained by introducing fluctuation on deposition rate in facet $s1$; (b)Evolution of lengths of facets with respect to thickness of the shell (T). Figures embeded are the zoomed-in figures of evolution of lengths of the corresponding facets with respect to T for $T \geq 9$.

facets {112} on the core, the influences of $R(= F_s/F_t)$, F_t and l_{ti} on the configuration of the shell can be summarized as follows:

1. For a thickness of the shell (T) large enough, there are two configurations of the shell, hexagonal and kinetic Wulff shapes with $l_s : l_t \approx \Delta F_s : \Delta F_t$.

2. When $R \in (\cos\theta, \sec\theta)$ (or $R \in (0.866, 1.155)$), the lines $F_t = C/l_{ti}$ where $C = 6D\bar{\Omega}|\lambda|/(1 - R\cos\theta)$ obtained by theoretical analysis give almost exact estimation of the critical values of (l_{ti}, F_t) for transition from a shell with six facets to a shell with twelve facets when T is large enough (see Fig. 8,9,10).

3. Given a value of $R \in (1, \sec\theta)$ (or $R \in (1, 1.155)$), this line is also a good estimate of the location of (l_{ti}, F_t) which can get ridge structures in which the small facets {112} evolve slowly within a certain thickness of the shell ("Y" shape with ridge structure).

4. Comparing results in Fig. 9 and Fig. 10, it is easier to get "Y" shapes in the direction {112} on the shell with R closer to $\sec\theta$ for $R \in (1, \sec\theta)$. Similarly, comparing results in Fig. 8 and Fig. 9, it is easier to have "V" shapes in the direction {112} of the shell with smaller R.

5. Influences of the values of R on the configurations of the shell can be summarized as follows:

   a. when $R \in (0, \cos\theta]$, the configuration of the shell is hexagonal;

   b. when $R \in (\cos\theta, 1]$, the shell is a hexagon or a do-decagon with "V" shapes in the direction {112};

   c. when $R \in (1, \sec\theta)$, the configuration of the shell is hexagonal, or "Y" shapes with ridge structures or "V" shapes in direction {112}, especially, when $R \lesssim \sec\theta$, the shell is a hexagon or a do-decagon with "Y" shapes in the direction {112};

   d. when $R \in [\sec\theta, \infty)$, the configuration of the shell is hexagonal.

6. Fluctuation of deposition rate on a single facet will result a quantum dot/wire on a single facet.

4.3. Influence of polarity of facets sa and facets sb

As suggested in some experiments in Zheng et al. (2013), the polarity of the planes {112} introduces three-fold symmetric structure on the shell, even though the core is six-fold symmetric. In our model, the polarity of the facets {112} are introduced by varying lengths of facets {112} on the core, surface energies and diffusion coefficients on facets {112}sa and {112}sb. In the following, the influence of lengths of facets {112} on the core, surface tensions and diffusion coefficients on the geometrical structure on the shell are investigated.

Table 2: Dimensionless parameters taken in the numerical simulations in Sec. 4.3

Sim.	$F_a[V_0]$	$F_b[V_0]$	$F_t[V_0]$	$l_{ai}[L_0]$	$l_{bi}[L_0]$	$l_{ti}[L_0]$	$D_a\bar{\Omega}$	$D_b\bar{\Omega}$	$D_t\bar{\Omega}$	γ_{sa}/γ_t	γ_{sb}/γ_t
#3.1	1.595	1.595	1.45	1.0	1.0	13	0.1169	0.1169	0.1169	3	2
#3.2	1.595	1.595	1.45	1.0	1.0	13	0.3339	0.2226	0.1113	3	3
#3.3	1.430	1.430	1.30	1.1	1.0	13	0.1113	0.1113	0.1113	3	3

4.3.1. Different surface tensions, $\gamma_{sa} \neq \gamma_{sb}$

Take $\gamma_{sa} = 3\gamma_t$ and $\gamma_{sb} = 2\gamma_t$ as a representative case for $\gamma_{sa} \neq \gamma_{sb}$. We start by assuming the diffusion coefficients on different facets are equal, i.e., $D_a = D_b = D_t = 0.1169$. The deposition rates on facet sa and facet sb are equal, i.e., $F_a = F_b = 1.595$ and $F_t = 1.45$. The core has six-fold symmetric structure with $l_{ai} = l_{bi} = 1$ and $l_{ti} = 13$ (see Simulation #3.1 in Table 2).

The configuration of the shell obtained by numerical simulation is shown in Fig. 12(a). In the numerical result, when the thickness of the shell increases from 0 to 9.40, l_{sa} is in the range of 1.0746 ± 0.16 and l_{sb} is in the range of 1.4049 ± 0.40 (see Fig. 13(a)). Therefore, different surface tensions on facets $\{112\}sa$ and $\{112\}sb$ play essential roles in the nanowire growth. It introduces asymmetrical structure on the shell of the nanowire. Moreover, the facets $\{112\}$ with larger surface tensions naturally tend to have smaller thicknesses. This conclusion is also consistent with the analytical results obtained in Sec. 3.1.3. Fig. 15(a), for a given thickness of the shell, shows that l_{sa}/l_{sb} behaves monotonically with regard to γ_{sa}/γ_{sb}. Larger asymmetry in surface tension on planes $\{112\}$ composed by facets $\{112\}sa$ and $\{112\}sb$ leads to larger asymmetry on geometrical structure of the shell on planes $\{112\}$.

Moreover, when the thickness of the shell is large enough which implies $\mathcal{N} \ll 1$, the ratio of the lengths of facets sa and sb first decreases because of the difference of λ_a and λ_b and then increases to $1(= \Delta F_{sa}/\Delta F_{sb})$ whereas l_{sa}/l_t and l_{sb}/l_t tend to $0.2(\approx \Delta F_{sa}/\Delta F_t = \Delta F_{sb}/\Delta F_t)$ (see Fig. 14(a)) because of deposition dominance at large $\mathcal{N}$. Numerical results mentioned above are consistent with the analytical results obtained in Sec. 3.2.

4.3.2. Different diffusion coefficients, $D_a \neq D_b$

Take $D_a = 3D_t$ and $D_b = 2D_t$ as a representative case for $D_a \neq D_b$ with $D_t = 0.1113$. The surface tension on the facets $\{112\}$ are equal to each other, i.e., $\gamma_{sa} = \gamma_{sb} = 3\gamma_t$. The deposition rates on facet sa and facet sb are equal, i.e., $F_a = F_b = 1.595$ and $F_t = 1.45$. The core has a six-fold symmetric structure with $l_{ai} = l_{bi} = 1$ and $l_{ti} = 13$ (see Simulation #3.2 in Table 2). It is found that different diffusion coefficients on facets $\{112\}sa$ and $\{112\}sb$ also introduces geometrical asymmetry in the shell. However, compared with

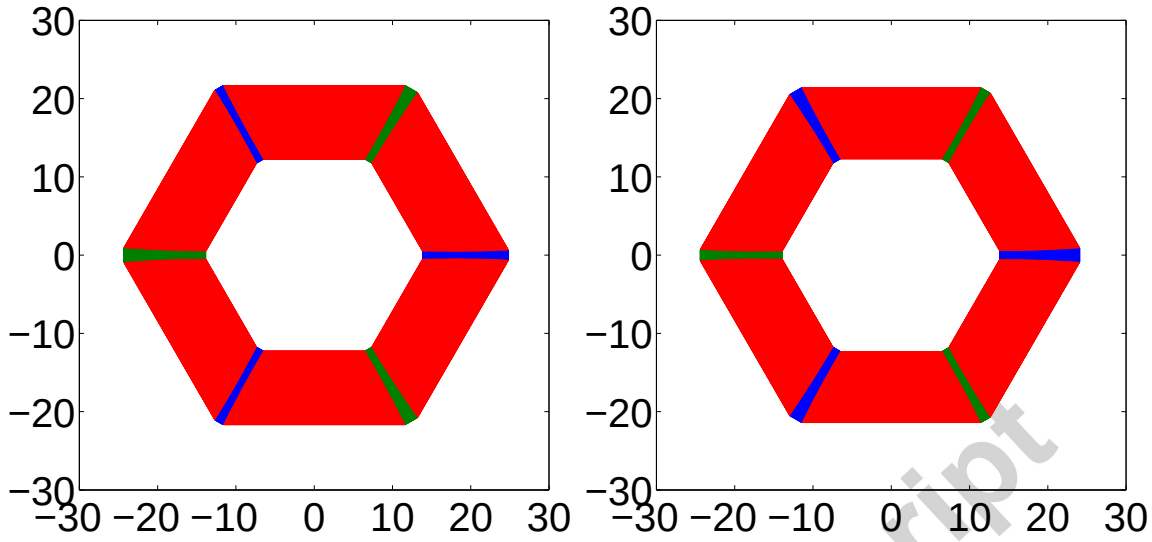

(a) (b)

Figure 12: Cross-section of the three-fold symmetric core-shell nanowire (facets $\{112\}sa$ with blue color, facets $\{112\}sb$ with green color and facets $\{110\}$ with red color). (a) The configuration of a core-shell nanowire with a six-fold symmetric core in Simulation #3.1 in which $\gamma_{sa} = 3\gamma_t$ and $\gamma_{sb} = 2\gamma_t$; (b)The Configuration of a core-shell nanowire with a three-fold symmetric core in which $l_{ai} = 1.1$ and $l_{bi} = 1$ in Simulation #3.3.

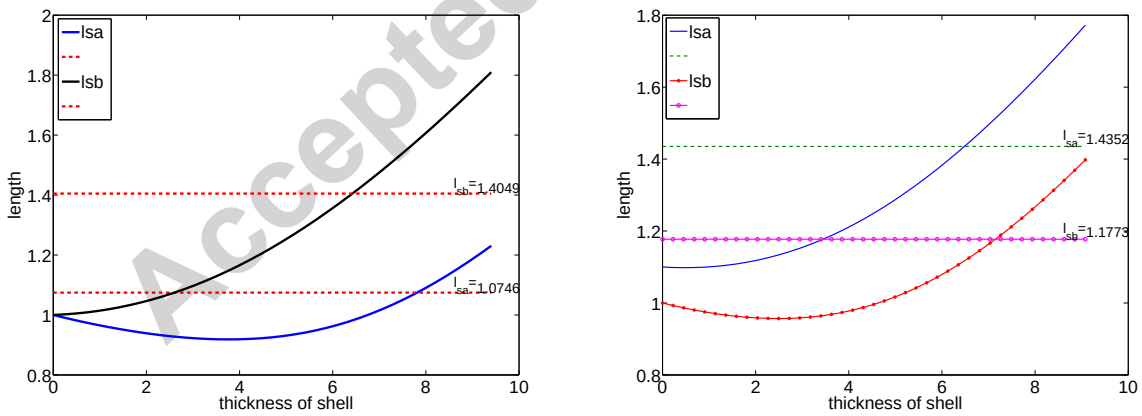

(a) (b)

Figure 13: (a) Evolution of $l_{sa}[L_0]$ and $l_{sb}[L_0]$ with respect to thickness of the shell ($T[L_0]$) in Simulation #3.1; (b) Evolution of l_{sa} and l_{sb} with respect to thickness of the shell (T) in Simulation #3.3.

the influence of different surface tensions, the influence of different diffusion coefficients is smaller with the parameters taken in this section. In Fig. 15(b), given a thickness of the shell, l_{sa}/l_{sb} behaves monotonically with regard to D_a/D_b. Larger asymmetry in surface diffusion coefficients on the planes {112} composed by facets {112}a and {112}b leads to larger asymmetry on geometrical structure of the shell.

Moreover, when thicknesses of the shell are large enough which implies $\mathcal{N} \ll 1$, the evolution is again dominated by deposition so that the ratios of length of facets sa to length of facets sb first decrease because of the difference of D_a and D_b and then increase to $1(= \Delta F_{sa}/\Delta F_{sb})$ whereas l_{sa}/l_t and l_{sb}/l_t tend to $0.2(\approx \Delta F_{sa}/\Delta F_t = \Delta F_{sb}/\Delta F_t)$ (see Fig. 14(b)). Numerical results mentioned above are consistent with the analytical results obtained in Sec. 3.2.

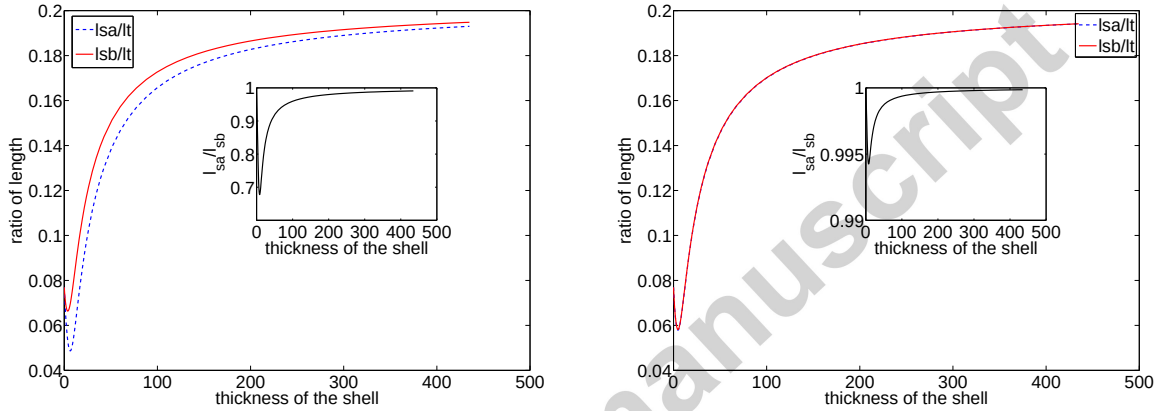

Figure 14: Evolution of l_{sa}/l_t and l_{sb}/l_t with respect to thickness of the shell (T). The figure embedded shows evolution of l_{sa}/l_{sb} with respect to thickness of the shell (T). (a) Numerical results obtained in Simulation #3.1; (b) Numerical results obtained in Simulation #3.2.

4.3.3. Different lengths of sa and sb on the core, $l_{ai} \neq l_{bi}$

Take $l_{ai} = 1.1$ and $l_{bi} = 1$ as a representative case for $l_{ai} \neq l_{bi}$ and $D_a = D_b = D_t = 0.1113$. The surface tensions on the facets {112} are equal to each other, i.e., $\gamma_{sa} = \gamma_{sb} = 3\gamma_t$. The deposition rates on facet sa and facet sb are equal, i.e., $F_a = F_b = 1.43$ and $F_t = 1.3$ (see Simulation #3.3 in Table 2). In the numerical result, when the thickness of the shell increases from 0 to 9.08, l_{sa} is in the range of 1.4352 ± 0.34 and l_{sb} lies in the range of 1.1773 ± 0.22 (see Fig. 13(b)). It is found that different lengths of {112}sa and {112}sb on the core also introduces geometrical polarity on the nanowire. It keeps the asymmetrical structure on the shell the same as the unsymmetrical structure on the core. Moreover, when the thickness of the shell is large enough which implies $\mathcal{N} \ll 1$, the ratio of lengths of facets sa and facets sb first increases and decreases to $1(= \Delta F_{sa}/\Delta F_{sb})$ whereas the ratio of l_{sa} to l_t and ratio of l_{sb} to l_t tend to be equal to $0.2(\approx \Delta F_{sa}/\Delta F_t = \Delta F_{sb}/\Delta F_t)$ (see Fig. 16(a)) due to deposition dominance. In Fig. 16(b), the growth rates of $(l_{sa} - l_{sb})$ decrease as $(l_{ai} - l_{bi})$ increase and the growth rates of $(l_{sa} - l_{sb})$ go to 0 when the thicknesses

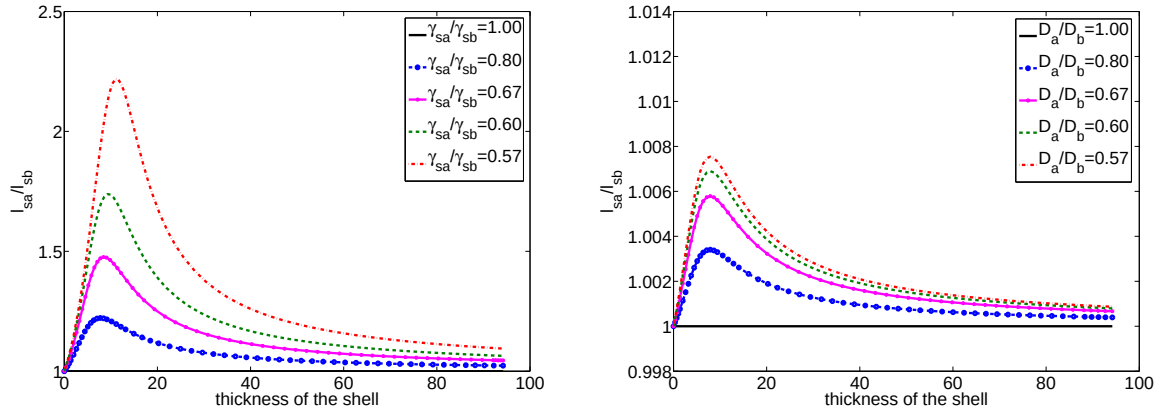

(a) (b)

Figure 15: Evolution of l_{sa}/l_{sb} with respect to thickness of the shell (T). (a)Numerical results obtained with different ratios of surface tensions on facets sa and facets sb; (b) Numerical results obtained with different ratios of diffusion coefficients on facets sa and facets sb.

of the shells are large. Numerical results mentioned above are consistent with the analytical results obtained in Sec. 3.1 and Sec. 3.2.

5. Conclusions

In this paper, a two-dimensional model has been proposed that accounts for capillarity and deposition in the cladding of faceted nanowires of pure materials. The growth processes and morphological evolution of shells around hexagonal cores (six facets {112} in the corners of six equivalent facets {110}) are investigated both analytically and numerically. Despite the fact that the model describes a pure material, the results accurately describe the experimental observations in alloy systems in facet formation and phase configuration.

The influence of polarity in planes {112}, due to the varying of surface energies, diffusion coefficients or lengths of facets {112} on the core, is investigated. Because of the competition between diffusion and deposition, at early times, facets {112} with larger surface energies or smaller lengths on the core or larger diffusion coefficients tend to have smaller thicknesses of the shell, given equal deposition rates on the facets {112}.

In addition, the deposition-dominant processes give rise to kinetic Wulff constructions. Deposition-dominant processes are important because they are not only common in experiments but also describe the long-time behaviors of large nanowire growth. Finally, it is shown analytically that there does not exist a "self-limiting" length on any facet in the dynamic processes for the configurations considered in this paper.

More specifically, the shape of the shell is governed by a competition between surface diffusion and

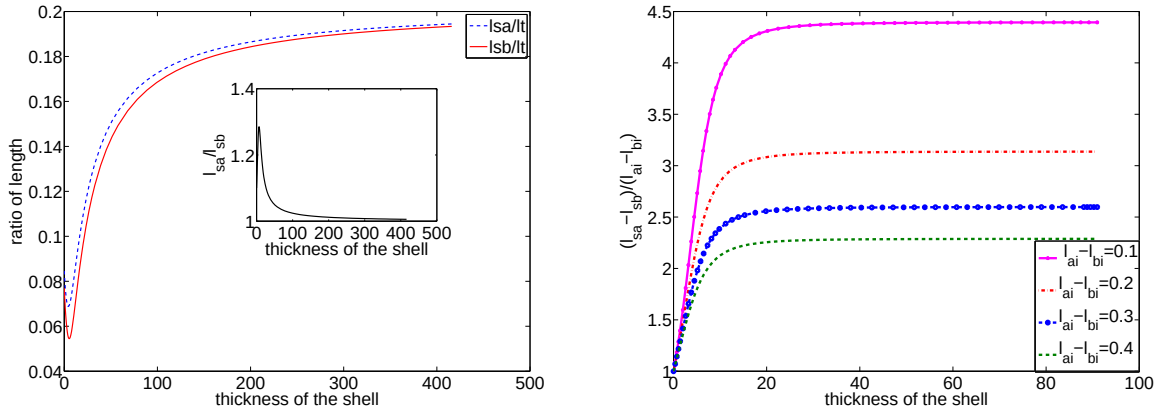

(a) (b)

Figure 16: (a) Evolution of l_{sa}/l_t and l_{sb}/l_t with respect to thickness of the shell (T) in Simulation #3.3; The figure embedded shows evolution of l_{sa}/l_{sb} with respect to thickness of the shell (T). (b) Evolution of $(l_{sa} - l_{sb})/(l_{ai} - l_{bi})$ with respect to thickness of the shell in Simulation #3.3.

deposition. The influence of surface diffusion scales as $1/(d_0 + 2T\sec\theta)$ where $d_0 = [2l_{ti} + \sec\theta(l_{ai} + 1)]$ is the dimensionless diameter of the core (scaled by the length of facets $\{112\}sb$ on the core, L_{bi}) and T is the thickness of the shell. Thus, for sufficiently small core diameters, the core is given by the equilibrium or surface-energy-controlled Wulff shape. However, as T increases from zero, if deposition rates are large enough, capillarity and diffusion will become less important and the shape can be completely controlled by deposition giving the kinetic Wulff shape. If the two shapes differ, then there is a transition from one shape to another.

The kinetic Wulff shapes are scale independent, or are self-similar. This implies that the kinetic Wulff shapes set the relative lengths of the facets but not their absolute sizes. If the shape is given by the kinetic Wulff shapes, then as T increases the sizes of all the facets must increase. Thus, in the kinetic Wulff shape limit, this would lead to V-like shapes of the regions within the shell behind the facets $\{112\}$ as shown in Fig. 6(b). Because the kinetic Wulff shape dominates at large sizes, the small facets must increase in size as the shell increases in size, and there can be no self-limiting facet size.

However, as was shown, during the transition between the equilibrium Wulff and kinetic Wulff shapes, it is possible for the small facets $\{112\}$ to evolve slowly with time. Thus, for a given set of deposition and materials parameters and a judiciously chosen wire diameter, it is possible for most of the growth of the shell to be in a region where the facets $\{112\}$ appear to have a fixed length. However, because the kinetic Wulff shape is different than the equilibrium Wulff shape, the length of the facet must eventually increase as T increases. It is this sometimes-rapid change in length as the kinetic Wulff shape is approached that can lead to a dot-like region of Al in the AlGaAs core as shown in Fig. 3(b).

In general, according to the numerical results, one finds three types of configurations characterized by the stripe shapes in direction {112} of the shell in the nanowire, i.e., the hexagon, the "Y" shape and the "V" shape (see Figs. 3(a), 3(b), 6(b), 6(a)). In particular, shells of nanowires with "Y" shapes and "V" shapes in direction {112} are considered to be associated with the formation of quantum dots/wires. Moreover, we compare our numerical results with the experimental results and observe quantitative agreement.

The influence of deposition rates on the configuration of the shell is investigated in detail. With parameters mentioned in Sec. 4.2 , if $F_t \cos\theta < F_s \leq F_t$ (or $0.866 < F_s/F_t \leq 1$), shells of nanowires have two possible configurations: the hexagon and the "V" shape (see Fig. 8). If F_s/F_t is in the interval $(1, \sec\theta)$ (or $(1, 1.155)$), the shell of the nanowire has three possible configurations: the hexagon, the "Y" shape and the "V" shape (see Fig. 9). As F_s/F_t approaches $\sec\theta$, only the hexagon and the "Y" shapes are present in the configuration of the shell (see Fig. 10). If $F_s/F_t \leq \cos\theta (\approx 0.866)$ or $F_s/F_t \geq \sec\theta (\approx 1.155)$, the shell is hexagonal. More specifically, regimes of deposition rates and diameters of the core introducing different configurations of the shell are generated numerically (see Figs. 8, 9, 10).

Finally, numerical results suggest that the polarity of crystal structures in planes {112} drives the growth of core-shell heterostructures with three-fold symmetric shells. Moreover, larger polarity on planes {112} composed by facets $\{112\}sa$ and $\{112\}sb$ will lead to larger asymmetry on geometrical structures of the shells on planes {112} (see Figs. 15(a), 15(b), 16(b)). As the sizes of the shell becomes large, capillarity becomes small and the kinetic process becomes deposition dominant. Under such conditions, the configuration of the shell is controlled by the deposition rates on the different facets.

In summary, a new model has been developed which describes the dynamic processes of the shells surrounding faceted nanowires. Mechanisms of stripes and quantum-dot formation in the shells of core-shell nanowires are identified. The predictions of the model quantitatively describe the influence of experimental parameters on the configurations of the shells of the nanowires, and so provide detailed guidance to future experiments.

Acknowledgments

This research was supported by the Office of Naval Research under Grant No. N00014-14-1-0697.

Appendix A. Derivation of average chemical potential

As suggested by Eq. (6) in Carter et al. (1995), the average chemical potential on facet i equals weighted curvature on the facet, κ_i^γ,

$$\kappa_i^\gamma = \frac{\int_0^{L_i} \mu_i(s) ds}{L_i}, \tag{A.1}$$

while κ_i^γ can be can be got by measuring changing in energy with respect to volume by moving the facet in a virtual distance.

Indeed, consider it on facet i, we set a Cartesian coordinate system by taking the middle point of facet i as its origin, the outer normal direction of facet i as positive y-axis, the direction parallel to facet i and pointing to the right hand side of the original point as positive x-axis. The neighboring facet of facet i lying on the right hand side of original point is denoted as facet $(i+1)$ while the neighboring facet of facet i lying on the left hand side of original point is denoted as facet $(i-1)$. Notice here, $i-1$, i and $i+1$ are not necessary the same as what we ordered in Sec. 2.1. Here, they are just notations which are introduced for expression convenience on calculating average chemical potential of each individual facet. Therefore, in this coordinate system, the outer normal direction of facet i, facet $i+1$ and facet $i-1$ can be denoted as $\mathbf{n}_i = (0,1)$, $\mathbf{n}_{i+1} = (n_{i+1}^x, n_{i+1}^y)$ and $\mathbf{n}_{i-1} = (n_{i-1}^x, n_{i-1}^y)$. The expressions of the lines on which facet i, $i+1$ and $i-1$ are lying in the Cartesian coordinate system mentioned above are given as follows,

facet i: $y = 0$ for $-\frac{L_i}{2} \le x \le \frac{L_i}{2}$;
facet $i+1$: $y = -\frac{n_{i+1}^x}{n_{i+1}^y}(x - \frac{L_i}{2})$;
facet $i-1$: $y = -\frac{n_{i-1}^x}{n_{i-1}^y}(x + \frac{L_i}{2})$.

The surface energy which is influenced by the facet i is $E = \gamma_i L_i + \gamma_{i+1} L_{i+1} + \gamma_{i-1} L_{i-1}$. We move facet i in its outer normal direction with a small distance h, then the energy difference introduced by moving right end of facet i and left end of facet i are in the following respectively.

$$\Delta E_r = \pm(\gamma_i \frac{n_{i+1}^y}{\sqrt{1-(n_{i+1}^y)^2}} - \gamma_{i+1} \frac{1}{\sqrt{1-(n_{i+1}^y)^2}})h, \tag{A.2}$$

$$\Delta E_l = \pm(\gamma_i \frac{n_{i-1}^y}{\sqrt{1-(n_{i-1}^y)^2}} - \gamma_{i-1} \frac{1}{\sqrt{1-(n_{i-1}^y)^2}})h \tag{A.3}$$

where $+$ is taken if facet $i+1$ or facet $i-1$ is located on the positive half plane, i.e., $y > 0$ and $-$ is taken if facet $i+1$ or facet $i-1$ is lying on the negative half plane, i.e., $y < 0$. Moreover, the volume difference introduced by small movement of facet i is

$$\Delta V = L_i h + O(h^2). \tag{A.4}$$

Therefore,

$$\begin{aligned}\kappa_i^\gamma &= \lim_{h\to 0} \frac{\Delta E}{\Delta V} = \lim_{h\to 0} \frac{\Delta E_r + \Delta E_l}{\Delta V} \\ &= \frac{1}{L_i}[\pm(\frac{\gamma_i n_{i+1}^y}{\sqrt{1-(n_{i+1}^y)^2}} - \frac{\gamma_{i+1}}{\sqrt{1-(n_{i+1}^y)^2}}) \pm (\frac{\gamma_i n_{i-1}^y}{\sqrt{1-(n_{i-1}^y)^2}} - \frac{\gamma_{i-1}}{\sqrt{1-(n_{i-1}^y)^2}})].\end{aligned} \tag{A.5}$$

In other words,

$$\bar{\mu}_i = \frac{1}{L_i}(\pm\frac{\gamma(\mathbf{n}_i)\mathbf{n}_i \cdot \mathbf{n}_{i+1} - \gamma(\mathbf{n}_{i+1})}{\sqrt{1-(\mathbf{n}_i \cdot \mathbf{n}_{i+1})^2}} \pm \frac{\gamma(\mathbf{n}_i)\mathbf{n}_i \cdot \mathbf{n}_{i-1} - \gamma(\mathbf{n}_{i-1})}{\sqrt{1-(\mathbf{n}_i \cdot \mathbf{n}_{i-1})^2}}). \tag{A.6}$$

References

Biasiol, G., Gustafsson, A., Leifer, K. and Kapon, E., 2002. Mechanisms of self-ordering in nonplanar expitaxy of semiconductor nanostructures. Phys. Rev. B 65, (205306)1-15.

Cahn, J. W. and Carter, W. C., 1996. Crystal shapes and phase equilibria: a common mathematical basis, Metallurgical and Materials Transactions A 27, 1431-1440.

Garcke, H., 2013. Curvature Driven Interface evolution. Jahresbericht der Deutschen Mathematiker-Vereinigung 115, 63-100.

Carter, W. C., Roosen, A. R., Cahn, J. W. and Taylor, J. E., 1995. Shape Evolution By Surface Diffusion and Surface Attachment Limited Kinetics on Completely Faceted Surface. Acta Metall. Mater. 43, 4309-4323.

Carter, W. C., Taylor, J. E. and Cahn, J. W., 1997. Variational Methods for Microstructureal-Evolution Theories, JOM 49, 30-36.

Cermelli, P., Friend, E. and Gurtin, M. E., 2005. Transport relations for surface integrals arising in the formulation of balance laws for evolving fluid interfaces. J. Fluid Mech. 544, 339-351.

Gurtin, M. E., 2008. Configurational forces as basic concepts of continuum physics. Springer II. Series 137.

Heiss, M., Fontana, Y., Gustafsson, Wüst, A. G., Magen, C., O'Regan, D. D., Luo, J. W., Ketterer, B.,Conesa-Boj, S., Kuhlmann, A. V., Houel, J., Russo-Averchi, E., Morante, J. R., Cantoni M., Marzari, N., Arbiol, J., Zunger, A., Warburton, R. J. and Morral, A. Fontcuberta i, 2013. Self-assembled quantum dots in a nanowire system for quantum photonics. Nat. Mater. 12, 439-444.

Jiang, N., Gao, Q., Parkinson, P., Wong-Leung, J., Mokkapati, S., Breuer, S., Tan, H. H., Zheng, C. L., Etheridge, J. and Jagadish, C., 2013. Enhanced minority carrier lifetimes in GaAs/AlGaAs core-Shell nanowires through shell growth optimization, Nano Lett. 13, 5135-5140.

Niu, X., Stringfellow, G. B., Lee, Y.-J. and Liu, F., 2012. Simulation of self-assembled compositional core-shell structures in $In_xGa_{1-x}N$ nanowires. Phys. Rev. B 85, (165316)1-5.

Porter, D. A. and Easterling, K. E., 1981. Phase transformations in metals and alloys. Chapman and Hall.

Rudolph, D., Funk, S., Döblinger, M., Morkötter, S., Hertenberger, S., Schweickert, L., Becker, J., Matich, S., Bichler, M., Spirkoska, D., Zardo, I., Finley, J. J., Abstreiter, G. and Koblmüller, G., 2013. Spontaneous Alloy Composition Ordering in GaAs-AlGaAs Core-Shell Nanowires. Nano Lett. 13, 1522-1527.

Shenoy, V. B., 2011. Evolution of morphology and composition in three dimensional fully faceted strained alloy crystals. J. Mech. Phys. Solids 59, 1121-1130.

Spencer, B. J., Voorhees, P. W. and Tersoff, J., 2001. Morphological instability theory of strained alloy film growth: the effect of compositional stresses and species-dependent surface mobilities on ripple formation during epitaxial film deposition. Phys. Rev. B 64, (235318)1-31.

Stone, H. A., 1990. A Simple Derivation of the Time-Dependent Convective-diffusion Equation for Surfactant Transport along A Deforming Interface. Phys. Fluilds A 2, 111.

Vastola, G., Shenoy, V. B., Guo, J., Zhang, Y.-W., 2011. Coupled evolution of composition and morphology in a faceted three-dimensional quantum dot. Phys. Rev. B 84, (035432)1-7.

Wagner, J. B., Sköld, N., Wallenberg, L. R., Samuelson, L., 2010. Growth and segregation of $GaAs - Al_xIn_{1-x}P$ core-shell nanowires. J. Cryst. Growth 312, 1755-1760.

Xie, Q., Madhukar, A., Chen, P. and Kobayashi, N. P., 1995. Vertically self-organized InAs quantum box islands on GaAs(100). Phys. Rev. Lett. 75, 2542-2545.

Zheng, C., Wong-Leung, J., Gao, Q., Tan, H. H., Jagadish, C. and Etheridge, J., 2013. Polarity-Driven 3-Fold Symmetry of GaAs/AlGaAs Core Multishell Nanowires. Nano Lett. 13, 3742-3748.